Large Scale Electrostatic Actuation

by

Daniel Jacques Benhammou

Submitted to the Department of Mechanical Engineering
in partial fulfillment of the requirements for the degree of

Bachelor of Science in Mechanical Engineering

at the

MASSACHUSETTS INSTITUTE OF TECHNOLOGY

June 2002

Author .....
Department of Mechanical Engineering
May 10, 2002

Certified by .....
Neil Gershenfeld
Associate Professor of Media Arts and Sciences
Thesis Supervisor

Accepted by .....
Ernest E. Cravalho
Chairman, Department Undergraduate Thesis Committee

Large Scale Electrostatic Actuation

by

Daniel Jacques Benhammou

Submitted to the Department of Mechanical Engineering
on May 10, 2002, in partial fulfillment of the
requirements for the degree of
Bachelor of Science in Mechanical Engineering

Abstract

Increasing developments in micro technology manufacturing have pushed for smaller and more powerful microactuators. Electrostatic actuation evolved as a means to supply MEMS scale devices with such mechanisms characterized by high force to volume ratios and simple fabrication. The ease of producing these electrostatic drives have made them attractive for macroscopic actuation. As large-scale actuators, electrostatic motors offers the potential to be the first printable motors. The ability to rapidly design and iterate mechanisms of actuation is not currently available using any other technology. The electrostatic actuators discussed in this thesis involve a stator and a slider which can both be actively driven. Experiments showed that by tuning the frequency and amplitude of the driving signal, it is possible to attain reasonable force. This thesis explores the feasibility of large-scale electrostatic motors using simple and affordable fabrication processes.

Thesis Supervisor: Neil Gershenfeld
Title: Associate Professor of Media Arts and Sciences

Acknowledgments

"zoom went the car and we were off again..." –Jack Kerouac

This work could have never come about without the help of innumerable professors, colleagues and friends. In particular, I would like to thank Neil Gershenfeld for posing the original problem to me. In addition to providing endless support and guidance, he would always push me to new levels and encourage me to think and try new things just for the sake of doing them and he never let me give up. I would also like to particularly thank several graduate students in the physics and media group who are not only friends, but mentors. Jason Taylor provided endless support when my project seemed daunting and impossible but perhaps most importantly, opened my eyes to the world of Tacos Lupitas. Yael Maguire also assisted me in whatever ways I needed and could answer just about any question I could think to ask.

I would also like to thank Aram Harrow, Ben Recht, Susan Murphy-Bottari, Mike Houlihan and the rest of my colleagues in the physics and media group at the MIT Media Lab.

I would like to thank my parents for always offering their support and encouraging me to take challenges even in the face of adversity and for giving me the chances to do so. I would also like to thank my brothers Jeremy and David.

Thanks to my friends, particularly Ian Parker, Jacob Beniflah, Asa Prentice, David Greenhouse and Aimee Ginley for always listening and giving feedback and support.

I could not have done this without your help.

Contents

List of Figures

List of Tables

Chapter 1

Introduction

Worldwide, nearly fifty percent of the electricity used each year powers electric motors [21]. In addition to electric motors, many other forms of actuation exist to provide rotation and translation in any way imaginable. Electrostatic actuators have recently become a mechanism of interest due to its ability to scale and actuate micro devices. The remarkable functionality when scaling and the simplicity of design which makes the use of electrostatic motors so promising.

All previous work focused on electrostatic actuation has been done on the microscale, but this thesis explores the possibility of printed motors by using simple designs of easily fabricated embedded electrode arrays. The ability to print motors offers an incredibly broad scope of applications. The arrays can be easily stackable to amplify force and since the motors are low current, dissipation is minimal. The added benefit of being able to print on flexible substrates adds to possibilities of actuating planar surfaces. From linear to rotational drive devices, electrostatic motors show promise in being the first printable actuators.

1.1 Outline

The first chapter is devoted to giving the reader an overview of different actuation mechanisms and motivations for electrostatics. The main forms of actuation, both macroscopic and microscopic are reviewed with brief explanations. Understanding actuation will help the reader appreciate the potential for electrostatic drives. This chapter concludes with an explanation of how macroscopic electrostatics have emerged from the micro electromechanical systems.

The second chapter in this thesis is devoted to background material. It begins by giving an explanation of the concepts behind electrostatics and then offers a brief overview of the

fundamental physics necessary to understand this work. After reviewing electric fields and potential, a rough performance estimate of an electrostatic motor is calculated. This estimate will help keep the rest of the work presented in perspective.

The third chapter focuses on single excitation electrostatic drives. This chapter is based primarily on experimental work on the subject. The chapter begins by focusing on electrode design and fabrication, continues to describe the equipment used in the experiment and finally ends with a description of a prototype device and results.

The fourth chapter continues along the trajectory of the single excitation electrostatics and introduces the dual excitation multiphase electrostatic drive or DEMED. This chapter starts with a finite element analysis of electrodes and then describes a controller for the motor. The chapter concludes with the hardware and prototype results.

The fifth chapter is a conclusion of the work described within these pages. It offers a discussion of the results from the experimentation and proposes further work on the subject of electrostatic motors.

In order to understand and truly appreciate the flexibility and utility of electrostatic actuation, it is important to have at least a loose understanding of alternate forms of actuation. This chapter is an overview of the main principles behind primary forms of both macroscopic and microscopic actuation.

1.2 Macroscopic Actuation

Macroscopic actuation is what most people think of when actuators come to mind. These mechanisms are the devices that surround us in our everyday lives. From the motor that drives your car, to the pump within your air conditioner. Everything that moves is driven by some sort of actuation. Even the muscles in your body are actuators and surprisingly good ones at that. This section reviews the principles behind some of the most common forms of macroscopic actuation: electromagnetic motors, combustors, hydraulics, pneumatics and muscles.

1.2.1 Electromagnetic Motors

Outside of bioactuators, electromagnetic actuation is the most common form of actuation around us today. Nearly every device that contains rotating mechanisms are driven by electromagnetic motors which contain a few key components: a rotor, a permanent magnet, and a coil. The rotor needs a torque to begin spinning which is achieved using electromagnetic forces. When a current is applied to the coil of the motor, a magnetic field is produced, which

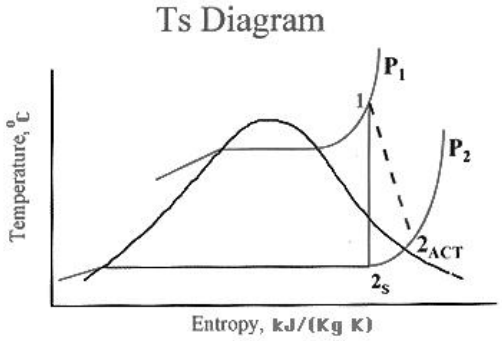

Figure 1-1: This figure shows the Temperature vs. Entropy diagram for a Brayton cycle.

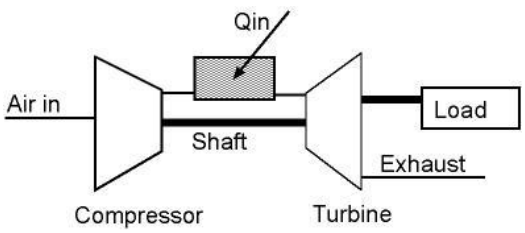

Figure 1-2: This figure shows the schematic of a typical Brayton cycle.

opposes the magnetic field of the permanent magnet thus generating a torque. As the motor turns, the poles of the electromagnet switch thereby keeping the rotor spinning [3].

1.2.2 Turbine and Combustion Actuation

A turbines is a device which converts the enthalpy and kinetic energy of a moving fluid into some form of mechanical work. Because of this, turbines have been used in many areas including steam power plants, jet engines, hydroelectric power plants, steam locomotives, among many others. A basic turbine consists of a rotor or series of rotors. These rotors are mainly composed of fins connected to a shaft. When a fluid flows through the fins, the angle of the fins causes the rotor or rotors spin, which causes the shaft to rotate. The torque in the shaft is then able to do some form of mechanical work, such as rotate a compressor or turn a generator which produces current.

Water, air and other gases are typical working fluids for a turbine. Early and most readily recognizable applications of a turbine are the windmill and water mill which harness moving air and water respectively and convert it into some form of useful work such as supplying the energy to grind grain or saw lumber. An important application is the steam power plant which utilizes steam pressure to rotate a generator and produce electricity [11].

Combustion engines work on the same principles as turbines except they usually use gases as the working fluid. A gas is injected and then undergoes a rapid heat transfer from the combustion of fuels and oxidizers. The Brayton cycle seen in figures 1-1 and 1-2 is a standard model for a combustion engine. The enthalpy and kinetic energy of the gas is then converted into mechanical energy by working against a piston or other surface causing actuation.

1.2.3 Hydraulics

The most common type of hydraulic actuators are hydraulic cylinders. These actuators usually are simple a piston using an incompressible fluid as the working fluid. Powerful motors put the working fluid under high pressure and the force it into a cylinder where all the surfaces are fixed except for on. The incompressible nature of the fluid makes these actuators extremely efficient and allows them to be some of the strongest that are readily available [13].

1.2.4 Muscles as Actuators

The most abundant actuator is also one with the highest force per volume ratio: muscle. This biomaterial is unique because it uses sugar as a form of energy; unfortunately it is extremely hard to maintain outside a living organism. Muscle cells are specialized for contraction and have high densities of actin microfilaments and myosin - proteins that control actuation. Smooth muscle cells are usually long and spindle-shaped. The cells are arranged in sheets, and individual cells in the sheets are in electrical contact with one another through gap junctions. This connection allows action potentials that are generated in the membrane of individual muscle cells to spread throughout the sheet. Each muscle fiber is composed of myofibrils - bundles of contractile filaments made up of actin and myosin. The cells use adenosine tri-phosphate, a molecule created in the mitochondria of the cell, to provide the necessary energy for actuation when triggered by an electrical impulse from the nervous system [19].

1.3 Microscopic Actuation

Recently, the development of microelectromechanical systems or MEMS have created the need for microactuators. These actuators are primarily on the millimeter or micron scale but extend down to the nanometer range. Devices requiring these microactuators range from optical switching to object manipulation.

1.3.1 Polysilicon Flexure Structures

Magnetic mictroactuation is a relatively new area of actuation that has already shown promising results [22]. One of the main advantages about using polysilicon flexure structures is that they can be batch-fabricated as opposed to manual assembly. The magnetic actuation combines electroplated NiFe films with surface-micromachined polycrystalline silicon. This

combination of materials provides new opportunities for actuated-structure designs and has already shown its ability to outperform electrostatic microactuators. Control of the magnetic field also allows significant actuation both in and out of the plane [12].

1.3.2 Shape Memory Alloy Micro-Actuation

In contrast to other actuators, actuation by means of shape memory alloys only utilize one component. Current research by Nanomuscle Inc. has developed an actuator that is simply a strand of a titanium-nickel alloy [6]. When current is passed through the wire, energy is dissipated in the form of heat and the alloy undergoes thermal expansion and shape change. Upon cooling, the alloy once again assumes its original shape. Problems with current shape memory alloys for actuation include the fact that many of the alloys have a low cycle life. The cyclic nature of thermal strain causes fatigue which will in turn cause the actuator to fracture [2]. Another disadvantage of using thermal control for actuation is the slow response time depending on heat transfer conditions. Despite these disadvantages, shape memory alloys offer 15 times higher work output per unit volume than hydraulic actuators [17].

1.3.3 Micro Actuator Arrays

Microfabricated actuator arrays have recently been developed for distributed micro manipulation. Some of the most recent developments involve an organic ciliary array of thin-film polymide bimorph microactuators using both electrostatic and thermal control to implement tasks [5]. These arrays use ciliary micro actuation to perform the tasks of part translation, rotation, orientation and centering. The idea employed by using the micro actuator arrays is using the theory of programmable vector fields to take advantage of the massively parallel manipulation [4]. The part being manipulated by the actuator array has an equilibrium state that may be predicted and cascaded using a sequence of fields to bring the part to a desire final state. The possible applications involve micro manipulation, however this technology is limited to very small scale actuation.

1.3.4 Electrostatic Actuation

Presently, most of the work in the field of electrostatic actuation is in the area of microactuation. Many of these applications are developing motors occupying and area less than 1mm^2. One of the main factors inhibiting the widespread use of these microdevices is the presence of frictional forces that dominate their dynamic behavior. In order to overcome friction, some micromotors have been designed using resonate circuits driven by radio-frequency a.c.

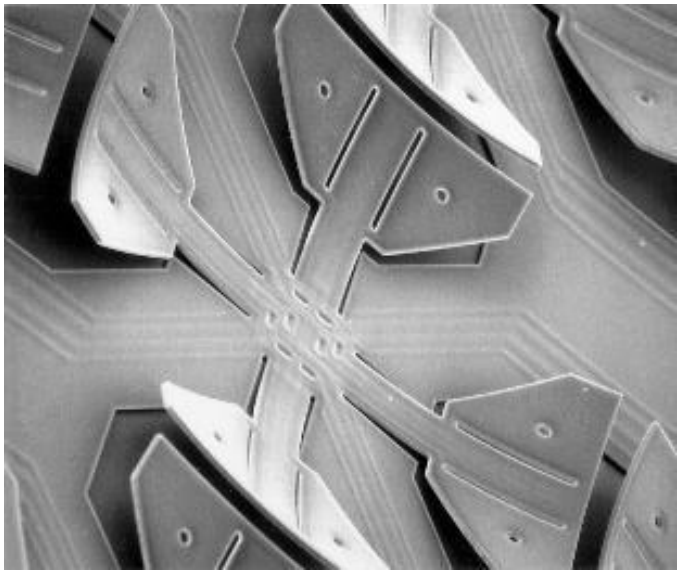

Figure 1-3: Four actuators in a common center configuration make up a motion pixel [7]

voltage to achieve stable levitation using open-loop control [10].

One of the most powerful electrostatic microactuators developed has been the dual excitation multiphase electrostatic drive which will be the foundation for much of the work presented in this thesis. The principle of this is that two arrays of electrodes are each driven by three-phase voltage to generate a linear force. These devices have been pushed by miniaturization and have shown to have an extremely high power to weight ratio. While the power of a single stator/slider combination may be low, stacking layers of electrodes has shown to scale the force linearly [26].

1.4 Scaling - Bridging the Gap

One of the unique properties of electrostatic actuators is that they scale remarkably well. Motors using electrostatic principles to generate their force can be used on either the microscopic scale or the macroscopic scale. The scaling of these motors works well since a large electrostatic drive is the same in principle as linking many microactuators with their outputs aggregated [15]. Research on these devices have shown that the power to weight ratio increases as the dimensions decrease, which makes electrostatics extremely promising as microactuator [16]. On the macroscopic scale, electrostatics also have a great deal of potential due to the ease of fabrication and their linear nature.

The scaling nature of electrostatic actuators is one of the biggest advantages over different

forms of actuation. The force given by an electrostatic motor is directly proportional to the number of electrodes driving the array. The added benefit of having printed motors increases the versatility of these actuators immensely. Designing an actuator could be as simple as specifying the number of electrodes and their configuration and then printing the motor with a special printer. The flexibility also greatly improves over most rotational motors used today. Since arrays of electrodes can be printed on flexible substrates, any planar surface could become an actuator. This thesis explores the implementation of macroscopic electrostatic actuation.

Chapter 2

Electrostatic Principles

The principles behind electrostatic actuation are similar to almost all forms of actuation: a condition is set upon two components, one of which being fixed, that creates an instability. In order to reestablish stability, the component which is not fixed moves and the cycle is repeated. For electrostatic motors, high voltage signals are applied which generate forces causing the slider to move in relation to the stator. What follows is in introduction to the underlying physics behind electrostatic actuation.

2.1 Electrostatics

One of the primary differences between classical electromagnetic motors and electrostatic motors is that stationary charges drive electrostatics while flowing charge drives electromagnetics. This differences makes electrostatic motors so promising. Unlike electromagnetic motors, the electrodes making up and electrostatic motor can be much more resistive without wasting energy through dissipation. The electrodes can also be placed on nearly any smooth surface making any pair of parallel surfaces a potential motor. This is due to the fact that electrostatic drives use high voltage and low current, so charge mobility is not of extreme importance. The ability to use resistive electrodes adds to the flexibility of electrostatics and the ease of fabrication.

2.2 Background Physics

Before going into the design and dynamics of the electrostatic systems discussed in this thesis, it is important to have an understanding of the underlying physics. While a background in basic electricity and magnetism is helpful, this thesis assumes no prior knowledge on the subject.

2.2.1 Coulomb Forces and Electric Fields

Electrostatic motors are based on and driven by the forces that act on charged particles. The interaction between these charges is described by Coulombs' law, which states that the force of attraction is proportional to the product of the charges and inversely proportional to the square of the distance between the two charges [18]. This equation can be written as

$$F = k\frac{q_1 q_2}{r^2} \tag{2.1}$$

where q_1 and q_2 are the charges of the two particles, r is the distance separating them and $k = \frac{1}{4\pi\epsilon_0}$ where ϵ is a constant called the permittivity of free space [8]. It seems deceivingly simple to say that this equation governs the system of an electrostatic drive, but nevertheless it is true. By using the principle of superposition, we can find the force on any charge resulting from the charges around it.

Suppose now that there exists a collection of charges, $q_1, q_2, \ldots, q_N$, that are all fixed in space. Each of these charges has a resulting force on an arbitrary particle with charge q_0. To determine the resulting force on the particle, the principle of superposition allows us to add all the forces which gives the force on q_0 as

$$\vec{\mathbf{F}}_0 = \sum_{j=1}^{N} \frac{q_0 q_j \hat{\mathbf{r}}_{0j}}{r_{0j}^2} \tag{2.2}$$

where $\hat{\mathbf{r}}_{0j}$ is a unit vector from the jth charge in the system to the charge q_0 [18]. By dividing out the charge q_0, we can define the electric field strength $\vec{\mathbf{E}}$ in newtons per coulomb. The resulting equation is

$$\vec{\mathbf{E}} = \frac{1}{4\pi\epsilon_0} \sum_{j=1}^{N} \frac{q_j \hat{\mathbf{r}}_{0j}}{r_{0j}^2}. \tag{2.3}$$

So far these equations and derivations have not revealed anything new, but they do help describe the system of charges. A system of charges also has a potential energy associated with it, which is the energy stored in the system configuration. Since we are assuming that the charges in the systems are static, we can use the electric field $\vec{\mathbf{E}}$ to determine the energy stored in the system. To find the energy, we must integrate over the entire volume of the electric field

$$U = \frac{1}{8\pi} \int_{Entire field} \vec{\mathbf{E}} \cdot \vec{\mathbf{E}} dv. \tag{2.4}$$

The energy within a system of charges will be of interest when determining the force of the electrodes on one another for electrostatic actuation.

2.2.2 Electric Potential and Capacitance

An important characteristic of an electric field is that the field is conservative. That is to say that for any points, P_1 and P_2 in and electric field $\vec{\mathbf{E}}$, the line integral

$$\int_{P_1}^{P_2} \vec{\mathbf{E}} \cdot d\mathbf{s} \tag{2.5}$$

has the same value, or the path is independent[9]. Since the vector field is conservative, we can define a scalar quantity, ϕ_{21} that is the work per unit charge between P_1 and P_2 without specifying a particular path. We use this to define the electric potential difference between the two points as

$$\phi_{21} = -\int_{P_1}^{P_2} \vec{\mathbf{E}} \cdot d\mathbf{s}. \tag{2.6}$$

The unit for electric potential in SI units is the volt. It is important not to confuse the electric potential difference, ϕ with the potential energy of an electric field U. The above derivations clearly show that an isolated system of charges Q where

$$Q = \sum_{j=0}^{n} q_j, \tag{2.7}$$

has a certain potential, ϕ. In this situation, the system of charges Q is in fact proportional to potential, ϕ. The constant of proportionality between the charge and the potential is defined as capacitance and is denoted by C in the relation

$$Q = C\phi. \tag{2.8}$$

The equation can easily be rearranged such that $C = Q/\phi$ to show the unit of capacitance is Coulombs per volt, or farad.

Capacitance is most often used in context of the potential difference between two surfaces. A capacitor consists of two parallel plates with a potential difference causing a capacitance. By putting a potential across the gap, charge collects on the two plates storing energy in the capacitor:

$$U = \frac{1}{2}C\phi^2. \tag{2.9}$$

The tendency of a system to move to a lower energy state causes the force needed for actuation.

2.3 Performance estimate

Many factors contribute to the performance of the electrostatic motor. Among the most crucial is the amplitude of the voltage used to drive the motor. In order to design an electrostatic drive such that the slider actually moves on the stator, it is important to derive the governing equations for the motor.

2.3.1 Capacitive Coupling

Since the basic structure of an electrostatic drive is a long array of parallel electrodes, it is not surprising that capacitive coupling exists between the electrodes as well as between the stator and slider. Since the width and the height of the electrodes are so much less than the length, the electrodes can be modeled as wires for determining the capacitance. We can simplify the task of analyzing the electrodes by looking at one pair of electrodes at a time.

The potential difference, ϕ placed on any two adjacent electrodes in fact causes the electrodes to behave as a capacitor. The equation of the capacitance of two horizontal parallel wires above the ground is

$$C = 0.1208l \left[\log_{10}\left(\frac{d}{a}\right) - \frac{d^2}{8h^2}\right]^{-1}, \tag{2.10}$$

where l is the length, d is the distance between the wires, a is the cross-sectional area, and h is the height of the wire above the ground [1]. Since the wires we are using for the electrodes are on the order of 100 microns or 10^{-4} meters and the distance above the ground is on the order of meters, we can disregard the $d^2/8h^2$ term as it is on the order of 10^{-8}. This leaves the simplified equation for the capacitance between any two adjacent electrodes as

$$C = 0.1208l \left[\log_{10}\left(\frac{d}{a}\right)\right]^{-1}. \tag{2.11}$$

By combining equations 2.11 and 2.8, the charge on the wire can be determined:

$$Q = 0.1208l \left[\log_{10}\left(\frac{d}{a}\right)\right]^{-1} \phi \tag{2.12}$$

Using the charge calculated in equation 2.12, the force can be applied by using Coulomb's Law, equation 2.1. The resulting force calculated is the force of two adjacent electrodes,

$$F = \frac{1}{4\pi\epsilon_0} \frac{\left(0.1208l \left[\log_{10}\left(\frac{d}{a}\right)\right]^{-1} \phi\right)^2}{r^2} \tag{2.13}$$

The driving force on the slider can be calculated by summing the forces over all the electrodes. To determine the forces, a matrix $\mathbf{F}$ can be defined as,

$$\mathbf{F} = \begin{bmatrix} f_{11} & f_{12} & \cdots & f_{1N_t} \\ f_{21} & f_{22} & \cdots & f_{2N_t} \\ \vdots & \vdots & \ddots & \vdots \\ f_{N_l1} & f_{N_l2} & \cdots & f_{N_lN_t} \end{bmatrix} \tag{2.14}$$

where N_t are the number electrodes on the stator and N_l are the number of electrodes on the slider. Since each electrode applies a force on every other electrode, calculating the force on a single electrode involves a double sum for the stator and slider and then subtracting duplicates,

$$F_{electrode} = \underbrace{\sum_{i}^{N_t}}_{stator} \underbrace{\sum_{j}^{N_l}}_{slider} f_{ij} - \underbrace{\sum_{i}^{N} f_{ii}}_{doublecounted} \quad . \tag{2.15}$$

.

Since the force dies off as $1/r^2$, the effect from the electrodes not in the immediate vicinity will have negligible forces and tend to cancel each other out, a simple calculation will be used to approximate the driving force. This approximation uses the number of electrodes actively involved in driving the slider must be multiplied by the force of each electrode. Typically, this will be the total number of electrodes N_{total} divided by the number of phases ψ since only one electrode per phase will generate an attractive force. This means that the number of electrodes contributing to the driving force at any one time is $N_{used} = \frac{N_{total}}{\psi}$. Multiplying the number of electrodes driving the motor by the force in equation 2.13 gives the new driving force on the slider:

$$F = \frac{1}{4\pi\epsilon_0} \frac{\left(0.1208l \left[\log_{10}\left(\frac{d}{a}\right)\right]^{-1} \phi\right)^2}{r^2} \left(\frac{N_{total}}{\psi}\right) \tag{2.16}$$

This is a rough estimate of the force generated by an electrostatic motor based on the analysis of two electrodes.

Another way to calculate the force is to evaluate the difference of the energy of the two states and then divide by the distance traveled since force can be determined by the difference in the energy between two states divided by the distance traveled:

$$F = \frac{dU}{dx}. \tag{2.17}$$

To calculate the energy, we must establish a capacitance matrix $\mathbf{C}$ such that

$$\mathbf{C} = \begin{bmatrix} c_{11} & c_{12} & \dots & c_{1N_t} \\ c_{21} & c_{22} & \dots & c_{2N_t} \\ \vdots & \vdots & \ddots & \vdots \\ c_{N_l1} & c_{N_l2} & \dots & c_{N_lN_t} \end{bmatrix} \tag{2.18}$$

where c_{ij} represents the capacitance between electrodes i and j. A similar matrix must be defined for the potential between electrodes,

$$\mathbf{\Phi} = \begin{bmatrix} \phi_{11} & \phi_{12} & \dots & \phi_{1N_t} \\ \phi_{21} & \phi_{22} & \dots & \phi_{2N_t} \\ \vdots & \vdots & \ddots & \vdots \\ \phi_{N_l1} & \phi_{N_l2} & \dots & \phi_{N_lN_t} \end{bmatrix} \tag{2.19}$$

Since each electrode applies a force on every other electrode, calculating the force on a single electrode involves a double sum for the stator and slider and then subtracting duplicates,

$$U_{electrode} = \underbrace{\sum_{i}^{N_t}}_{stator} \underbrace{\sum_{j}^{N_l}}_{slider} \frac{1}{2} C_{ij}\phi_{ij}^2 - \underbrace{\sum_{i}^{N} \frac{1}{2} C_{ii}\phi_{ii}}_{doublecounted} . \tag{2.20}$$

The energy from the electrodes not applying the direct force tend to cancel out so a simplified equation for the energy of the system can be used. Equation 2.9 gives the energy of a system of two electrodes. Applying 2.9 using the capacitance in equation 2.11, gives the equation for the energy for a pair of electrodes:

$$U = \frac{0.1208l}{2} \left[\log_{10} \left(\frac{d}{a} \right) \right]^{-1} \phi^2. \tag{2.21}$$

Combining equation 2.21 with equation 2.17 and multiplying by the number of active electrodes gives an approximation to the force applied by the electrode arrays:

$$F = \frac{0.1208lN_{total}}{2d\psi} \left[\log_{10} \left(\frac{d}{a} \right) \right]^{-1} \left(\phi_2^2 - \phi_1^2 \right) . \tag{2.22}$$

Using equation 2.13 and testing the capacitance of an experimental array of electrodes gives the projected force on a 300 electrode electrostatic drive as 2.5 millinewtons. This is further explored in Chapter 4 where a finite element analysis is described which also focuses on two electrodes.

Chapter 3

Single Excitation Drive

Single excitation drives are similar to dual excitation multiphase electrostatic drives or DEMEDs in that a three phase, high voltage signal is applied to initiate driving force. Unlike dual excitation drives however, only the stator is driven and the slider can be any dielectric material with low charge mobility. The general principle is to charge up a piece of dielectric material, and then cycle high potential across the electrodes embedded in the stator. Since the dielectric has low charge mobility, the charge on the electrodes provide both the repulsive and attractive force needed to drive the material.

3.1 Electrode Fabrication

For the single excitation electrostatic drive, little hardware is needed to facilitate actuation. Since the principle is to simply push a dielectric material across an array of embedded electrodes, the only hardware needed is a suitable array of electrodes and the driving electronics and software. Since flexibility and rapid iterations were essential in this process, it was important to develop a simple and economically efficient method of fabricating electrodes for the electrostatic drive.

3.1.1 Laser Cutting Mask

Fabricating the electrodes for both the single excitation drive and the dual excitation drive was non trivial. The main task, was finding a low cost method of fabricating electrodes with resolution on the order of hundreds of microns. The primary requirement for the electrodes is that a potential can be distributed equally over their length. This requirement allows a poor conductor to work as electrodes since the motion is driven by static and not dynamic charge.

Table 3.1: Optimal cut parameters

Parameter	Value
Speed	65%
Power	30%
Pulses Per Inch	200
Direction	y - axis
Cut Width	300μm

The first method of fabrication focused on using the laser cutter to generate masks for screen printing electrodes. Screen printing involves using a mask which is a pattern cut from a material, usually vellum, and then overlaying the pattern with a paint or ink. The first step in this process involves calibrating the laser cutter in order to optimize the power and speed to achieve the finest cut. Since the beam of the laser is not perfectly circular but elliptical, it was important to test the direction of the cut. To determine the optimal direction of the laser cut, a series of tests were performed varying the direction of the laser. The test cuts were then placed under a microscope which showed that the y-direction produced thinner cuts. The most influential factor in the quality of the cut, however, was focusing the laser on the mask material.

Unfortunately, with the particular laser cutter used for this operation, there is no absolute reference point in which to base the focal distance. The method of focusing rather involves cutting a single line in the y-direction and then changing the focal length by the smallest increment (0.01 inches) and cutting another line. This process was repeated 20 times on a 150 micron thick piece of vellum to achieve a large number of samples of varied cut quality. The vellum was then examined under a microscope and each line was measured to determine the width of the cut. The finest width cut by the laser cutter was 400 microns with the default power and speed parameters.

With the focal height optimized, the next step was to determine the optimal values for the speed, power and pulses per inch settings. By first setting the power and pulses per inch constant and varying only the speed, it was possible to make a series of cuts to determine the optimal values for the speed. This process was repeated for the power and pulses per inch to determine the optimal values for the critical parameters shown in table 3.1.

Using the values from table 3.1 for the parameters, the width of the final cut measured 300 microns. By optimizing the adjustable parameters for the narrowest cut, the mask could then be designed. The pattern involved lines in the y-direction, two-and-a-half inches in length

spaced out every 600 microns. The initial design was about two-and-a-half inches wide and consisted of roughly 200 electrodes. The first substrate tested with the mask pattern was a sheet of vellum. Unfortunately, in the process of cutting the substrate, the laser heated up the vellum causing it to shrink and become increasing brittle. The result of the shrinking was that the area between the electrodes became increasingly tensioned as more electrodes were ablated. As the tension grew, the vellum itself began to curve making the focal length obsolete.

The experiment proved that vellum would not be a suitable substrate for the electrode mask. The next material tried was a plastic sheet of standard transparency film. This substrate did not experience the shrinking as severely as the vellum, although it was still an issue. The main problem with using the plastic appeared when the laser instead of vaporizing the material, melted it enough so that gummy scallops formed on the areas separating the electrodes. After determining that this would not be appropriate as a mask, paper was tested as a substrate. The paper used did not display the problem of shrinkage like the other materials, but the mask was too fragile to use. In addition, one problem that all the substrates exhibited was that once cut, the electrodes of the mask could not be kept parallel without tensioning the mask to the point of breaking.

3.1.2 Laser Cutting Array

Due to the ease of designing patterns and the ease of fabrication, the laser cutter was once again employed to layout an electrode array. This time, an acrylic plastic substrate was used by having the electrode pattern directly ablated into the material. The principle behind this method of ablation was to leave the paper backing on the acrylic while the laser cut the electrode pattern. With the mask cut and the paper still on the acrylic, a conductive paint or spray could be applied covering the paper and the electrode pattern cut into the acrylic. After the conductive coating was dry, the paper could be removed, leaving the electrodes embedded in the acrylic.

Unlike cutting the mask from paper, transparency film or vellum, the acrylic maintained enough ridgedness so that it did not warp and the electrodes remained parallel. The first conductive coating applied was Electrodag 6C-54 by Acheson Colloids Company. This is a highly conductive nickel compound in a viscous fluid form. After the electrode pattern was cut, the Electrodag 6C-54 was applied with a brush and then coaxed into the laser-cut acrylic with a squeegee; then the sample was left to dry. Upon inspection the following day, it was discovered that the Electrodag 6C-54 reacted with the acrylic and had started to break down the plastic. The embedded electrodes became a mush of dissolved plastic and attempting to

remove the paper backing destroyed the acrylic base.

The next conductive coating used was Choshield 4900 by Chomics. This coating is packaged in an aerosol spray can for easy application. Unfortunately, the consistency of the aerosol is primarily fine metallic particles which weekly adhered to the substrate. This proved to be a problem once the paper backing was removed exposing the electrodes. When a high potential was applied across the electrodes, the metallic dust particles scattered between the embedded electrodes lowered the dielectric breakdown constant so shorts occurred across the array.

The last conductive coating tested was a can of traditional metallic spray paint. The spray PDS-92 Copper by Premium Decor was applied in the same way as the Choshield 4900 aerosol spray. The spray paint had much better adhesive properties and quickly bonded to the surface. The electrodes appeared to be in excellent form once the paper backing was removed from the acrylic, however the reflective particles used to give the paint a metallic appearance turned out to have low charge mobility. When using a multimeter to test the embedded electrode array, a potential could not be measured across the electrodes since the spray did not conduct charge at all.

One additional method of fabricating electrodes using the laser cutter was attempted. This trial involved directly ablating the electrode pattern from a conductive material. The material used for this was metalized mylar which has a resistance of approximately one ohm per square. Trying to directly cut the mylar does not yield promising results since the material is so reflective. The result of a cut is a rough, scalloped line with poor definition. In order to improve the cut quality, a dark piece of paper was weakly adhered to the metalized mylar. The paper helped to absorb the energy from the laser and resulted in a clean cut. The main problem with using this process as a means of fabricating the electrodes is that the air circulation within the laser cutter disturbs the cut electrodes so achieving a straight electrode is quite difficult.

3.1.3 Printing Electrodes

The next experiment performed to fabricate embedded electrode arrays consisted of using a normal laser printer. The idea behind this was that while the ink did not conduct, there might be enough charge mobility within the carbon of the ink to use as electrodes. The benefits of such a system would surpass any other process due to the ease of design and fabrication. Unfortunately, the printed electrodes had no conductive properties and no signal could be measured when a signal was applied on a printed electrode.

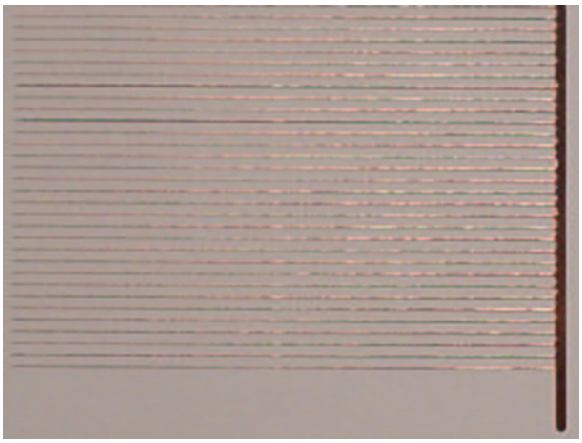

Figure 3-1: This figure shows a single phase of the embedded electrodes cut by the Roland vinyl cutter.

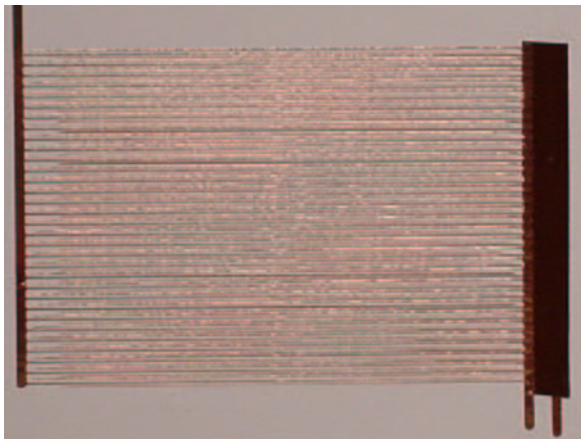

Figure 3-2: This figure shows the array of electrodes after all three phases have been transfered.

3.1.4 Vinyl Cutting Electrodes

The most successful technique for fabricating the embedded electrode arrays used a Roland vinyl cutter. This machine is simply a knife that is controlled in the X-Y plane and can either be down or up. The substrate for the electrodes was a roll of copper with an adhesive side backed with wax paper. The vinyl cutter lowers the knife and traces a pattern cutting only the copper and not the backing. With the design cut in the copper, the pattern can be transfered to any flat surface.

While the Roland vinyl cutter is a relatively straight forward and simple machine, designing the electrode arrays such that they turn out is nontrivial. The first step is to layout the design using the software package PCB Design and Make. This software allows easy layouts for simple geometries. In order to cut the smallest traces possible, we can change the line width within the software. The smallest line width available in the software is one mil; however the vinyl cutter cannot cut lines less than approximately 25 to 30 mils.

The first tests with the vinyl cutter involved laying out two of the three phases of electrodes together. The third phase was laid out by itself and then transfered and overlaid to complete the array of electrodes. Since these arrays were designed to push the spec limits of the machine, the electrodes were very thin and had a tendency to break. The main difficulty with these electrodes was removing the copper in the areas between the electrodes without peeling up the electrodes themselves.

After many marginally successful attempts, this approach was abandoned for a slightly

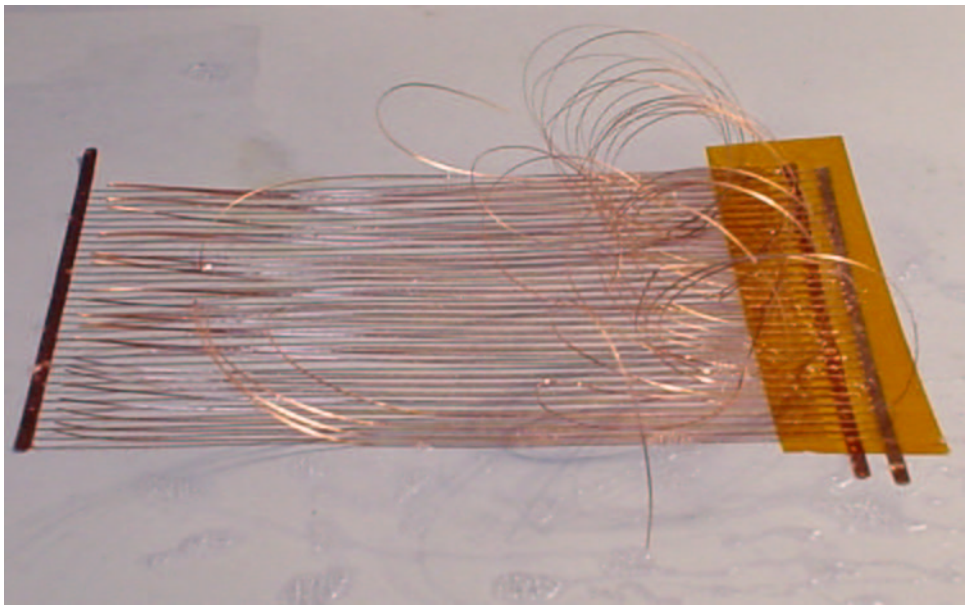

Figure 3-3: Copper electrodes curled as a result of dissolved adhesive.

more complicated but more promising one. The new technique involved cutting each of the three phases independently and then transferring them all to a surface to achieve the three-phase array. This technique proved to be time consuming but very successful.

3.1.5 Post Processing

Once the electrodes are fabricated, they are not completely ready for actuation. Immediately after fabrication, the electrodes have no insulation and are extremely susceptible to dielectric breakdown - particularly when charged on the stator. In order to provide a small amount of insulation without increasing the separation between the stator and the slider significantly, a dielectric spray is applied. The kind of spray used to provide insulation is critically determined by the method of fabricating electrodes. One of the best dielectric sprays used for electronic circuits is Konformal coating. Figure 3-3 demonstrates the results of using the Konformal dielectric coating on an array of electrodes cut by the vinyl cutter. The Konformal coating acted as a solvent, dissolving the adhesive holding the copper electrodes to the paper. As a result, a standard acrylic dielectric spray was applied in several coats to supply insulation.

Table 3.2: Parallel Port Output

Value	Output	Value	Output
0x00	0000	0x08	1000
0x01	0001	0x09	1001
0x02	0010	0x0a	1010
0x03	0011	0x0b	1011
0x04	0100	0x0c	1100
0x05	0101	0x0d	1101
0x06	0110	0x0e	1110
0x07	0111	0x0f	1111

3.2 Software

For a single excitation electrostatic drive, the software needed to drive the dielectric material across the embedded electrodes is very simple. The code can be broken up into two sections: charging the dielectric material and driving the material. Charging up the dielectric material involves simply charging a pair of electrodes for a given period of time which in turn causes charge to build up on the dielectric material. The driving phase involves cycling the potential on the electrodes to drive the dielectric material. Due to the simplicity of the operations, the parallel port works very well for controlling the drive and is included in the appendix A.1.

3.2.1 Parallel Port Code

By using a combination of the outputs shown in Table 3.2, it is possible to generate a three-phase driving square wave. As the code in Appendix A.1 show, the bits that must be used to drive the electrodes on the first three pins of the parallel port are: 0x06, 0x05, and 0x03. By cycling these bits with the parameters established and listed in Table 3.3, we get a a square wave driving function. Figure 3-4 illustrates the cyclic function driving the electrodes.

3.3 Drive Electronics

The optimal driving voltage for the electrostatic drive is of course to operate just within the specification limits of the system. For the electrodes, the limiting factor is the magnitude of the potential, ϕ between adjacent electrodes. The goal, therefor is to apply the maximum potential possible without achieving dielectric breakdown between the embedded electrodes.

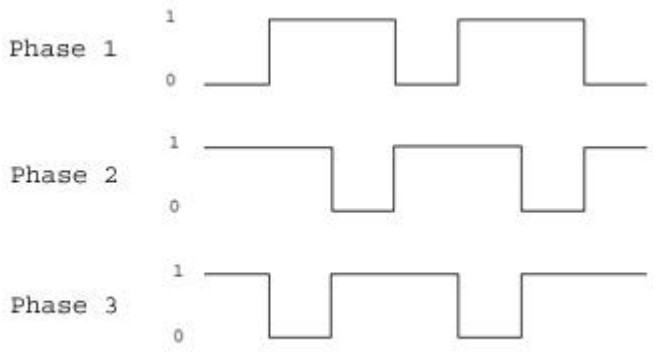

Figure 3-4: Square-wave driving function

Table 3.3: MAX233 input/output chart

MAX233 Input	MAX233 Output	Trek Output
0v	+12v	+750v
+5v	−12v	−750v

3.3.1 High Voltage Power Supplies

In order to use the signal provided by the parallel port, the voltage must be amplified. The voltage amplifiers used for this were two Trek 50/750 high voltage signal amplifiers. Each of the amplifiers has two channels capable of ±750 volts at a maximum of 50 milliamps. Each Trek amplifier was also tuned so that they would linearly amplify the input signal by 100 times such that an input of 5v would give an output of 500v.

3.3.2 Signal Processing

The outputs from the parallel port of PCs is based on TTL logic where a 1 is represented by 5 volts and 0 is represented by 0 volts. Sending the signal directly from the parallel port to the Trek 50/750 therefor limits the maximum potential from the amplifier to 500 volts. In order to take full advantage of the amplifier, it is necessary to map a digital one to at least 7.5 volts and a zero to −7.5 volts. To do this, a Maxim MAX233 multichannel RS-232 driver was used. This IC has a pin layout shown by Figure 3-5 and performs the mapping function shown by table 3.3.

Figure 3-7 shows the assembled typical operating circuit depicted in Figure 3-5. Figure 3-6 shows the additional hardware necessary to run the electrostatic drive and the experimental

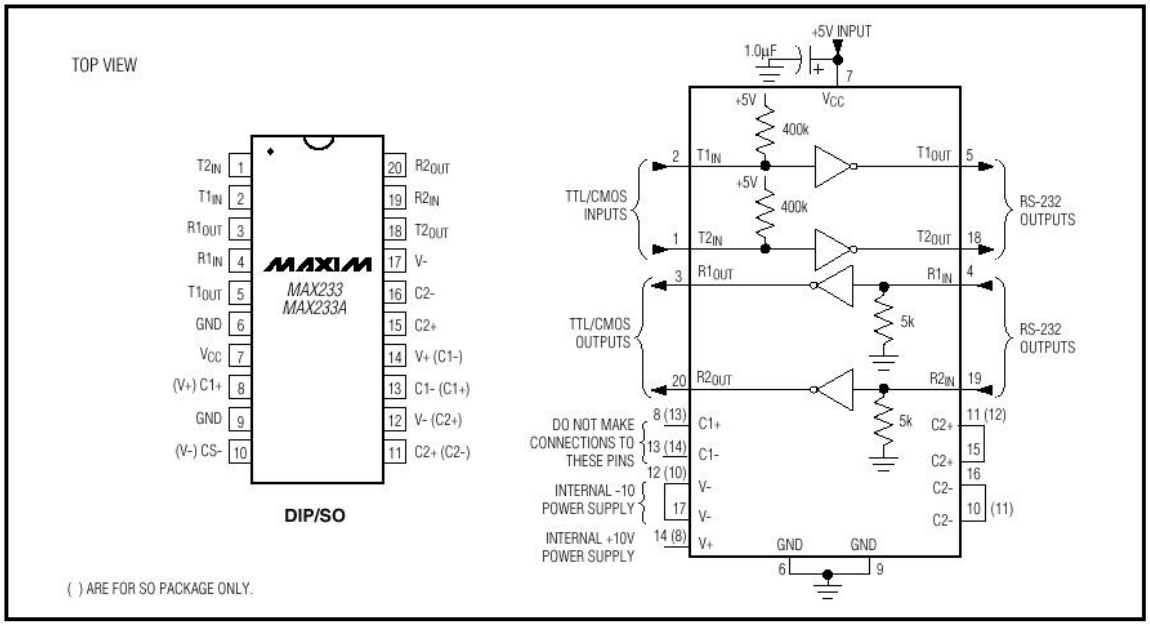

Figure 3-5: MAX233 pin layout and typical operating circuit [14]

configuration.

3.4 Prototype Drive and Experimental Results

The prototype of the single excitation electrostatic drive utilized an array of printed electrodes manufactured by SCA Paper. The electrodes themselves use a silver compound binded by a resin. Each individual electrode is half a millimeter wide and is separated by half a millimeter from adjacent electrodes. The array consists of 40 sets of 3-phase electrodes for a total of 120 electrodes. The dimensions of the array is 120 millimeters in the direction of motion and and 90 millimeters in the direction parallel to the electrodes.

The key parameters for driving the dielectric material across the array of electrodes were the time to charge the sample and the time per phase. After trying many different combinations, the first success involved using a small piece of paper as the dielectric material. The paper was 0.2 inches wide by 0.5 inches long and was place perpendicular to the electrodes. By using a charging time of 10 seconds and then cycling the three phase signal every 16 millisecond, the paper was able to jump across ten or so electrodes at a time when given an initial push. The critical parameters can be seen in Table 3.4.

The paper needed an initial push because the force acting on the sample was not enough to overcome the the static frictional force. In most of the experimental electrostatic motors,

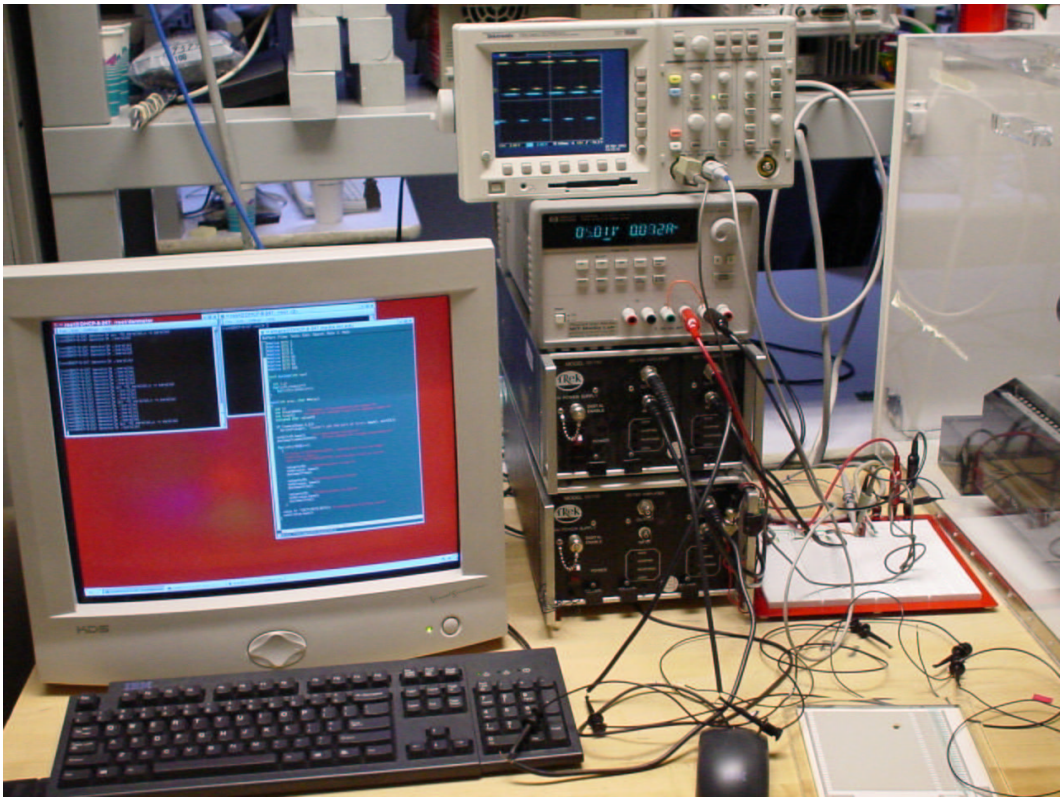

Figure 3-6: Experimental hardware for driving the three phase high voltage signal for actuation.

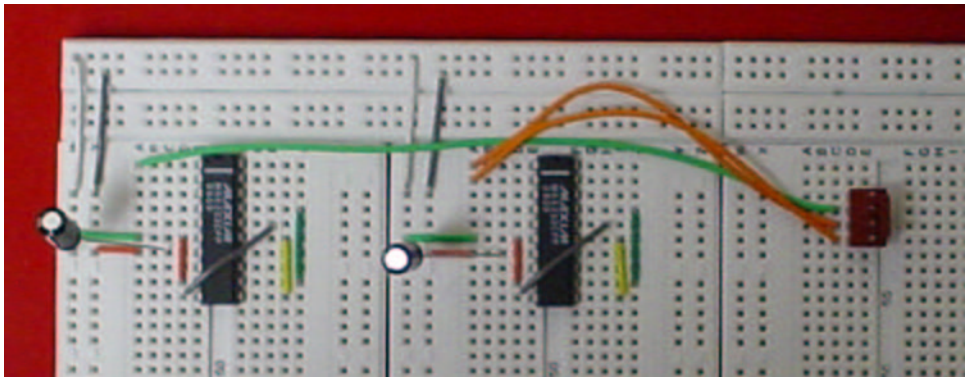

Figure 3-7: Mounted MAX233 signal amplification circuit

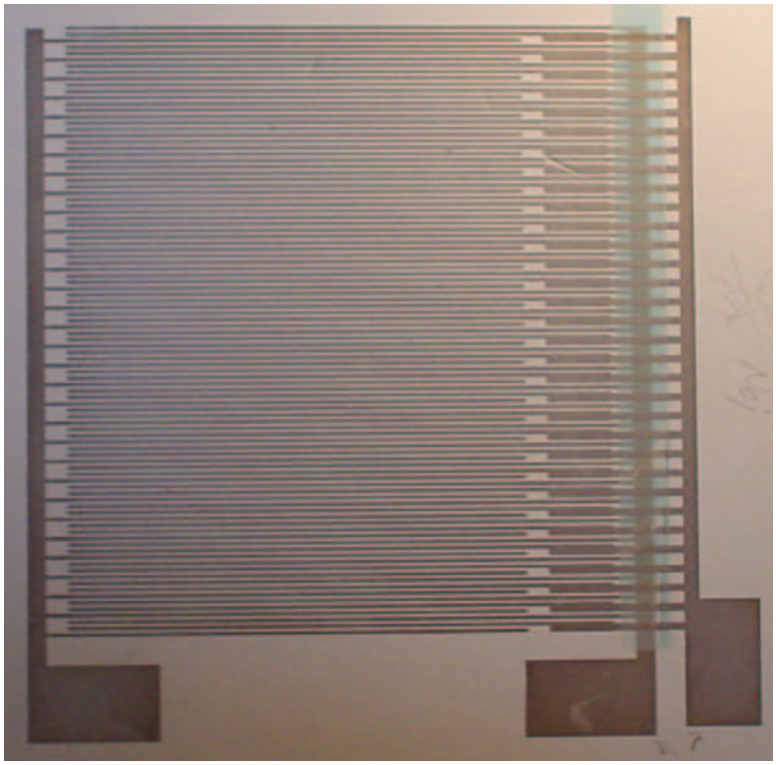

Figure 3-8: Array of printed electrodes

Table 3.4: Critical Parameters for Electrostatic Motion

Parameter	Value
Potential, ϕ	420 volts
Charge Time	10 seconds
Phase Delay	16 milliseconds
Frequency	21 Hertz

Table 3.5: Materials tested for single excitation electrostatic drive

Material	Dimensions	Results	Comments
Red Heat Shrink	5mm × 10mm	Jumps roughly 1cm On occasion jumps 2cm	too big?
Paper	5mm × 10mm	vibrates under voltage	friction?
Mylar	5mm × 10mm	no movement	May be too heavy
Rubber	5mm × 10mm	no movement	May be too
Transparency Film	5mm × 10mm	Jumps when pushed	friction?
Plastic Wrap	5mm × 10mm	Vibrates, moves when pushed	

a dielectric fluid was used to prevent breakdown between the electrodes but also to act as a lubricant. Most of the motors also used glass micro-spheres to reduce friction and help facilitate motion.

Using these studies as a model, glass micro-spheres were introduced to the array of electrodes to reduce friction. The micro-spheres used were class 5A microbeads from Cataphote Inc. with diameters between $105\mu\text{m} - 125\mu\text{m}$. Unfortunately, the spheres seemed to conduct charge and upon applying the voltage to the electrodes, dielectric breakdown was immediately observed.

Since we wanted to avoid using a dielectric fluid, we abandoned the use of the glass micro-spheres in favor of increasing the voltage. Since the Trek voltage amplifiers were linear, we had to vary the inputs to increase the potential between electrodes. To increase the potential, the signal processing circuit was designed and implemented as described in section 3.3.2. The new output from the Trek voltage amplifiers after introducing the circuit was over 800 volts. Unfortunately, the electrode arrays were not rated to such a high voltage and once again, dielectric breakdown could be observed. Figure 3-9 shows the result of dielectric breakdown between electrodes using the increased potential. In order to drive the dielectric material across the electrodes, it was essential to have the force between the stator and slider to be higher than the frictional force inhibiting motion. By using only small samples as the dielectric material being driven, the frictional forces were extremely small. The mass of the samples were all well below one gram and the surfaces were smooth. In order to determine the effect on the materials, several different samples were tested: paper, mylar, rubber, heat shrink, transparency film and plastic wrap. All of these samples were tested under the same conditions in table 3.4. The results are summarized in table 3.5.

Figures 3-10 through 3-14 show the progression of a dielectric sample moving across an array of embedded electrodes. The frequency of the signal driving the dielectric is close to

Figure 3-9: The result of dielectric breakdown between electrodes

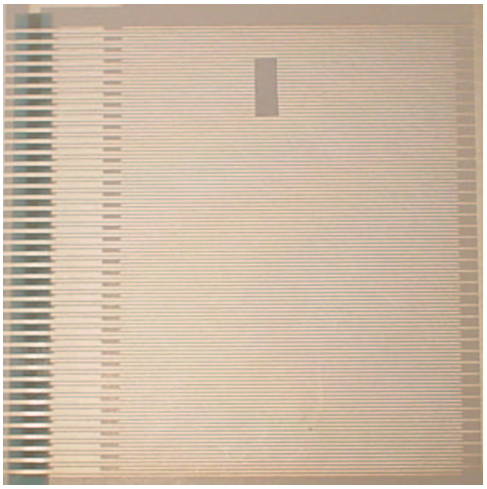

Figure 3-10: This figure shows a small piece of dielectric material at time $T = 0$ seconds.

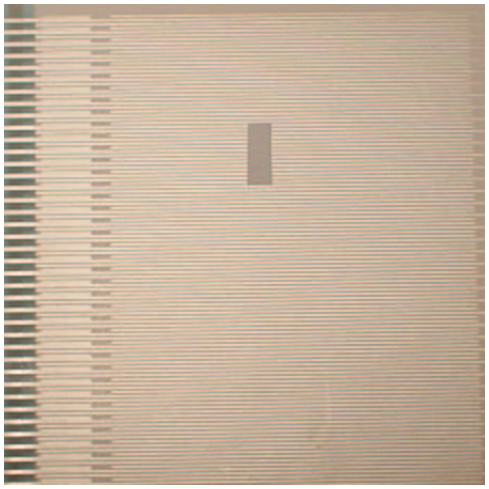

Figure 3-11: This figure shows a small piece of dielectric material at time $T = 2$ seconds.

20 Hertz and the images reflect movement over approximately 10 seconds. The dielectric material used in this test was a piece of paper with an area of roughly 50mm^2.

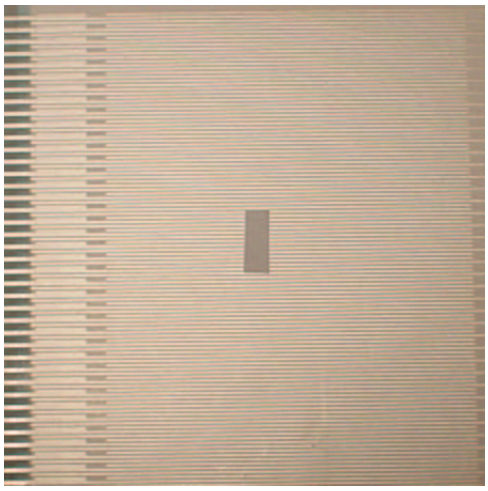

Figure 3-12: This figure shows a small piece of dielectric material at time $T = 4$ seconds.

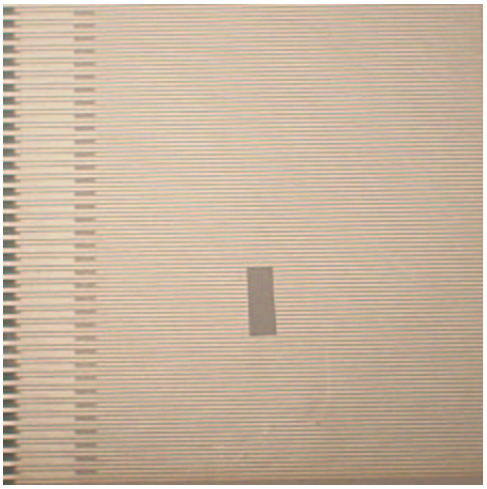

Figure 3-13: This figure shows a small piece of dielectric material at time $T = 6$ seconds.

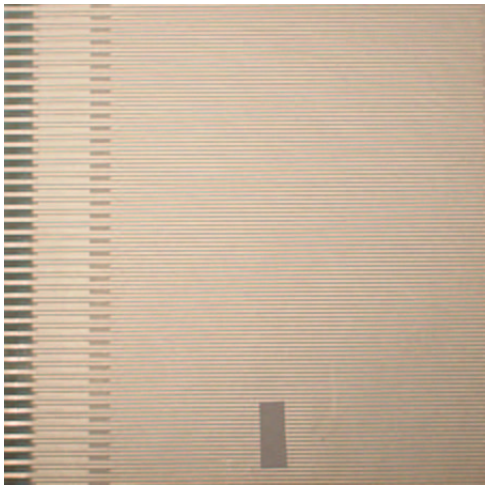

Figure 3-14: This figure shows a small piece of dielectric material at time $T = 8$ seconds.

Chapter 4

Dual Excitation Multiphase Electrostatic Drive

Dual Excitation Multiphase Electrostatic Drives or DEMEDs are very similar to single excitation electrostatic drives except that both the stator and the slider are actively driven. In almost all cases, the stator is driven by three-phase high voltage power whereas the slider can be driven by either three or four-phase potential. If a sinusoidal signal is driving the motor, a three-phase slider will suffice; however if positive square waves are driving the motor, a four-phase slider is needed to generate the force needed for motion [15].

4.1 Overview

This chapter focuses on DEMEDs, from theory to practice. The first section reviews a finite element analysis of two electrodes using the software package ANSYS. The following section describes a DEMED controller using a sinusoidal driving signal for a three-phase slider/stator combination. Given that the parallel port can only output digital signals, it is important to have means of driving an electrostatic drive by means of simulating a sinusoidal wave. The following chapter describes the algorithm used to digitally control a DEMED and then concludes with a prototyped device and results.

4.2 Finite Element Analysis

Electromagnetic simulations are critical to the development of any electric system. In order to get a better understanding of the forces and the electric field between stator and slider electrodes, a pair of such electrodes were modeled using ANSYS. ANSYS is an extremely

Table 4.1: ANSYS Simulation Parameters

Parameter	Value
Length	2μm
Width	2μm
Height	10μm
Potential (electrode 1), ϕ_1	-5v
Potential (electrode 2), ϕ_2	5v
Boundary Potential, ϕ_B	0v

powerful tool for modeling complex systems by mean of finite element analysis or FEA. Alex Wissner-Gross, an undergraduate at the MIT Media Lab did the following finite element analysis simulation of electrodes. Since many of the systems in real life have such complicated characteristics, solving implicitly is not always an option. For example, even a system as simple as modeling a pair of electrodes is extremely complicated considering the geometry and boundary conditions. FEA is a way to numerically solve systems given complex geometry and boundary conditions. ANSYS takes the given parameters and generates a mesh of points over the object being modeled. The software then uses the mesh to generate a solution for each point within it. By using a post processor, it is easy then to go back and evaluate any of the electromagnetic properties attributed to the system.

The first step in modeling the electrodes was to layout the geometry. To better understand the lower limits of the system, the geometry was modeled smaller than the actual test equipment. Each of the electrodes are modeled to be simple rectangles, two microns by two microns on an end with a height of 10 microns. The electrodes in the model are separated by a gap of four microns and offset also by four microns, which makes the total gap between electrodes $4\sqrt{2}$ microns. The potential, ϕ across the electrodes is 10 volts. An overview of the parameters in the model are given in table 4.1. An important note about the model is that it assumes as a boundary condition that the electric field at infinity is 0.

Figure 4-1 is a visual representation of the electric field in the x-direction as a result of the potential across the two electrodes. In all of models, the x-axes is the horizontal direction and the y-axes is the vertical. The model shows that the square geometry creates an unusual disturbance in the electric field. Since one electrode is at a positive potential and the other at a negative, this figure shows that the field is strongest at the corners of the electrodes nearest each other. Figure 4-2 is very similar to Figure 4-1, except this is a representation of the electric field in the y-direction.

Figure 4-3 is a visual representation of the electric potential around the electrodes. The

potentials illustrated in the figure are consistent with what is expected and could be approximated by the equation

$$\phi = -\int \vec{\mathbf{E}} \cdot d\mathbf{s}, \tag{4.1}$$

where $\vec{\mathbf{E}}$ is just

$$\vec{\mathbf{E}} = \frac{1}{4\pi\epsilon_0} \sum_{j=1}^{N} \frac{q_j \hat{\mathbf{r}}_{0j}}{r_{0j}^2} \tag{4.2}$$

from equation 2.3. As we expect, the potential is 0 along the line equidistant from both electrodes.

The figure of most interest is Figure 4-4, which shows the force on the electrodes given all the parameters in table 4.1. In this figure, ANSYS shows that the forces in the x-direction are on the order of 10^{-11} Newtons; however this calculation also assumes a potential of 10 between electrodes. A rough estimate based on Coulomb's law, equation 2.1 allows us to see how the FEA estimate scales. Since the voltage across the electrodes is two orders of magnitude greater, the distance is significantly less, and we are accounting for many more electrodes, the estimate for the force on a large-scale electrostatic motor is on the order of magnitude of 10^{-2} Newtons.

4.3 DEMED Controller

The most common method of driving three-phase electrostatic motors is the dual-frequency driving method [25]. This method involves applying two, three-phase voltages to the three poles of the slider and stator. The electrostatic force resulting from the potentials between the electrodes of the slider and stator generate the force which drives the motor. The displacement speed of the slider with respect to the stator can be determined by the frequencies of the driving voltage,

$$u = 3p(f_t - f_l) \tag{4.3}$$

where u is the velocity of the slider, p is the pitch of the electrodes, f_t is the driving frequency of the stator and f_l is the driving frequency of the slider.

4.3.1 Electrode Capacitance and Conductance

Since simply applying a potential across two electrodes itself will not cause a force, it is important to reestablish the principles of the electrostatic drive. The parallel electrodes of the stator and slider act like parallel wire capacitors. The potential difference between the

Figure 4-1: ANSYS model of electric field in the x-direction between two electrodes

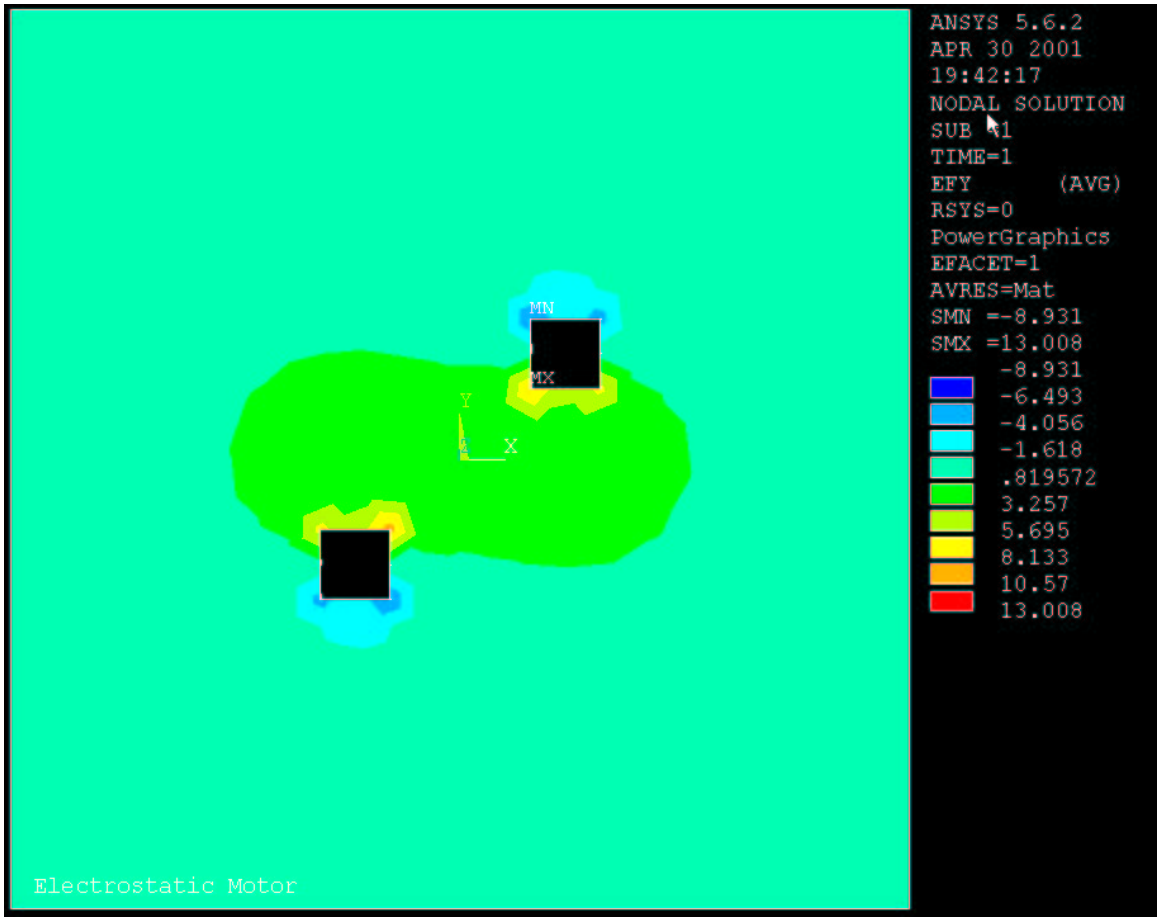

Figure 4-2: ANSYS model of electric field in the y-direction between two electrodes

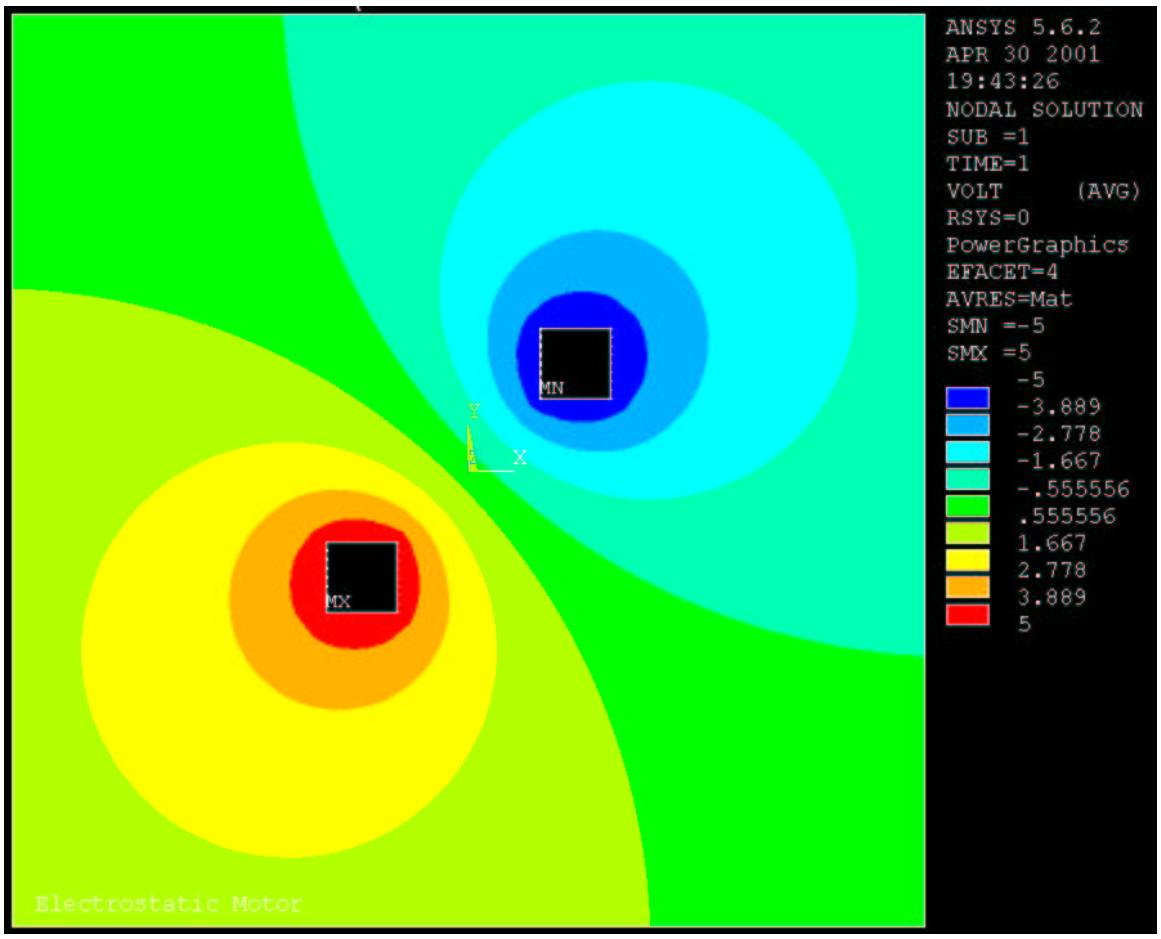

Figure 4-3: ANSYS model of potential between two electrodes

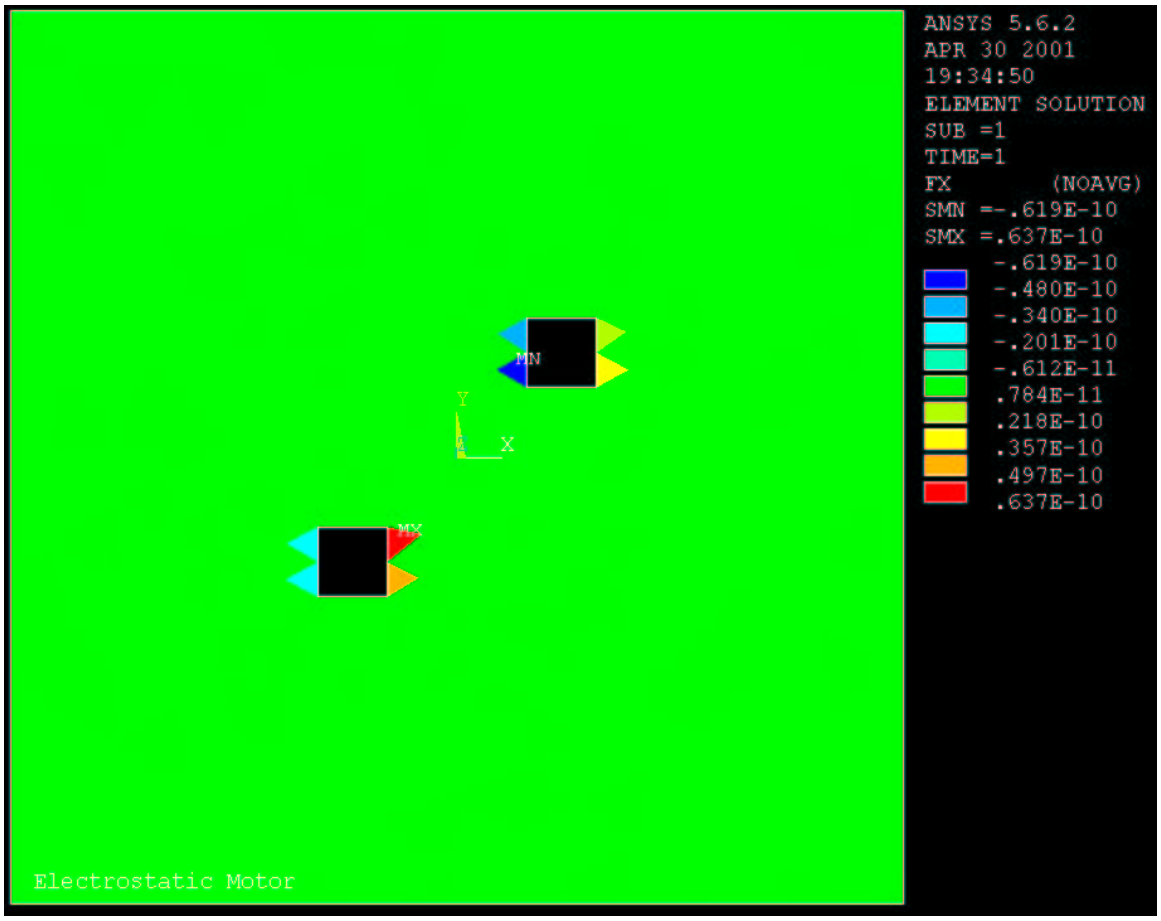

Figure 4-4: ANSYS model of force between two electrodes in the x-direction

two wires causes charge to build up, which in response causes an electrostatic force. It is this force that drives the motor.

Since the DEMED has a total of six poles and six independent phases, the system can be modeled as a six-terminal network. The dielectric loss within the network can be represented by the interconnections of capacitances and conductances. We can express the capacitance components of the network by using a 6×6 matrix $\mathbf{C}$ representing the capacitance coefficients:

$$\mathbf{C} = \begin{bmatrix} C_{st} & C_t & C_t & C_m^0 & C_m^+ & C_m^- \\ C_t & C_{st} & C_t & C_m^- & C_m^0 & C_m^+ \\ C_t & C_t & C_{st} & C_m^+ & C_m^- & C_m^0 \\ C_m^0 & C_m^- & C_m^+ & C_{sl} & C_l & C_l \\ C_m^+ & C_m^0 & C_m^- & C_- & C_{sl} & C_l \\ C_m^- & C_m^+ & C_m^0 & C_l & C_l & C_{sl} \end{bmatrix} \tag{4.4}$$

where $C_m^0 = C_0 + \cos(\theta_e)$, $C_m^+ = C_0 + \cos(\theta_e + \frac{2\pi}{3})$, and $C_m^- = C_0 + C_a\cos(\theta_e - \frac{2\pi}{3})$. The constants C_sl, C_st, C_l, C_t, C_0, and C_a are determined by the physical properties of the stator and slider [25]. θ_e represents the electric angle of the slider:

$$\theta_e = \frac{2\pi}{3p}x_e \tag{4.5}$$

where x_e is the position of the slider relative to the position of the stator.

The conductance components of the six-terminal network can likewise be expressed in terms of a 6×6 matrix $\mathbf{G}$. Due to the fact that each of the six arrays of electrodes are nearly identical, we can assume that the dielectric loss tangent ($\tan\delta$) is the same on every network path. This assumption lets us approximate the matrix $\mathbf{G}$ for a signal with frequency ω as

$$\mathbf{G} = \omega\tan\delta\mathbf{C}. \tag{4.6}$$

We can expand this to get

$$\mathbf{G} = \begin{bmatrix} \omega\tan\delta C_{st} & \omega\tan\delta C_t & \omega\tan\delta C_t & \omega\tan\delta C_m^0 & \omega\tan\delta C_m^+ & \omega\tan\delta C_m^- \\ \omega\tan\delta C_t & \omega\tan\delta C_{st} & \omega\tan\delta C_t & \omega\tan\delta C_m^- & \omega\tan\delta C_m^0 & \omega\tan\delta C_m^+ \\ \omega\tan\delta C_t & \omega\tan\delta C_t & \omega\tan\delta C_{st} & \omega\tan\delta C_m^+ & \omega\tan\delta C_m^- & \omega\tan\delta C_m^0 \\ \omega\tan\delta C_m^0 & \omega\tan\delta C_m^- & \omega\tan\delta C_m^+ & \omega\tan\delta C_{sl} & \omega\tan\delta C_l & \omega\tan\delta C_l \\ \omega\tan\delta C_m^+ & \omega\tan\delta C_m^0 & \omega\tan\delta C_m^- & \omega\tan\delta C_- & \omega\tan\delta C_{sl} & \omega\tan\delta C_l \\ \omega\tan\delta C_m^- & \omega\tan\delta C_m^+ & \omega\tan\delta C_m^0 & \omega\tan\delta C_l & \omega\tan\delta C_l & \omega\tan\delta C_{sl} \end{bmatrix} \tag{4.7}$$

4.3.2 Slider Thrust Force

To determine the thrust force acting on the slider, we examine the case in which we apply the voltage

$$\begin{aligned} \mathbf{v} &= \mathbf{v_t} + \mathbf{v_l} \\ &= v_0 \left[\sin(\psi_t), \sin(\psi_t - \tfrac{2\pi}{3}), \sin_t + \tfrac{2\pi}{3}), 0, 0, 0\right] + v_l \left[0, 0, 0, \sin(\psi_l), \sin(\psi_l - \tfrac{2\pi}{3}), \sin_l + \tfrac{2\pi}{3})\right] \end{aligned} \tag{4.8}$$

where the vector $\mathbf{v}$ represents the voltage on the poles and ψ_t and ψ_l express the phases of alternating current for the stator and slider respectively. The vectors $\mathbf{v_t}$ and $\mathbf{v_l}$ likewise are the stator and slider components of the driving voltage vector $\mathbf{v}$.

Using the principle of virtual work, the thrust force of the motor can be calculated as

$$\begin{aligned} f_x &= \tfrac{1}{2}\mathbf{v^t}\frac{\partial \mathbf{C}}{\partial x}\mathbf{v} \\ &= \tfrac{3\pi}{2p} C_a c_0 v_l \sin(\psi_t - \psi_l - \theta_e) \end{aligned} \tag{4.9}$$

Equation 4.7 clearly shows that the thrust force depends on many parameters. To simplify the control of the thrust force, we will establish the following condition for ψ_t, ψ_l and θ_e such that

$$\psi_t - \psi_l \theta_e = \frac{\pi}{2} \tag{4.10}$$

For further simplification and ease of control, we will assume that a three-phase sinusoidal wave with constant frequency and constant amplitude will drive the motor. This establishes that the phases of the stator signals are

$$\psi_t = \omega_0 t \tag{4.11}$$

where ω_0 is the frequency of the wave. Applying these conditions allows us to establish conditions that the slider signal should satisfy:

$$\psi_l = \omega_0 t - \theta_e - \frac{\pi}{2} = (\omega_0 - \omega_e)t - \frac{\pi}{2} \tag{4.12}$$

where ω_e is the angular velocity of the slider electrodes with respect to the stator electrodes ($\theta_e = \omega_e t$). Combining Eqs. 4.7 and 4.8, we obtain

$$f_x = \left(\frac{3\pi}{2p} C_a c_0\right) v_t. \tag{4.13}$$

If v_0 is kept constant, v_l is simply proportional to f_x, and we can easily control the thrust force by v_l alone.

4.4 Hardware

In order to have a functioning DEMED, substantial amount of hardware is needed. Some of the components are similar to that of the single excitation drive but many are different altogether. In addition to the extra array of electrodes for the slider, an air table was developed and fabricated to reduce friction between the stator and slider. The code driving the electrostatic motor is also different as is the signal processing equipment.

4.4.1 Air Table

Since repulsive forces cannot be obtained using strictly potentials and perfect conductors to drive the motor, it is necessary to achieve some other means of levitating the slider to reduce friction and generate motion. To achieve this, an air table was designed and fabricated for the purpose of being able to mount a specially designed stator such that upon pressurizing the air table, pin holes in the stator would provide an air bearing for the slider to hover on.

The air table consists of two pieces seen in figures 4-5 and 4-6. The base mounting plate (figure 4-5) is an 11 inch square of aluminum one inch thick. The plate also is fitted with 20 holes around the perimeter to secure the stator. A channel is machined into the plate to provide a port for a pressurized gas.

The top plate (figure 4-6) is also an 11 inch square of aluminum one quarter of an inch thick. This piece has an identical footprint to the base mounting plate with an additional cut of a nine inch square from the center. The volume created by the cut in the top plate creates a reservoir of high pressure gas which supplies the pinholes in the stator with gas. Since the velocity of the flow in the reservoir is orders of magnitude less than the flow through the stator, the reservoir can be modeled as having constant pressure.

4.4.2 Signal Processing

Signal processing for a DEMED differs somewhat from the single excitation circuitry because in addition to $+12$ volts and -12 volts, ground is also needed. Since there are three possible potentials, we will have to use two bits of data, A and B to control each phase. Table 4.2 illustrates the logic table needed for controlling each line of motor.

Figure 4-5: Top plate with square hole to maintain pressure reservoir

Figure 4-6: Base Mounting Plate

Table 4.2: Signal Processing Logic

A	B	Output
0	0	+12v
1	0	0v
1	1	−12v

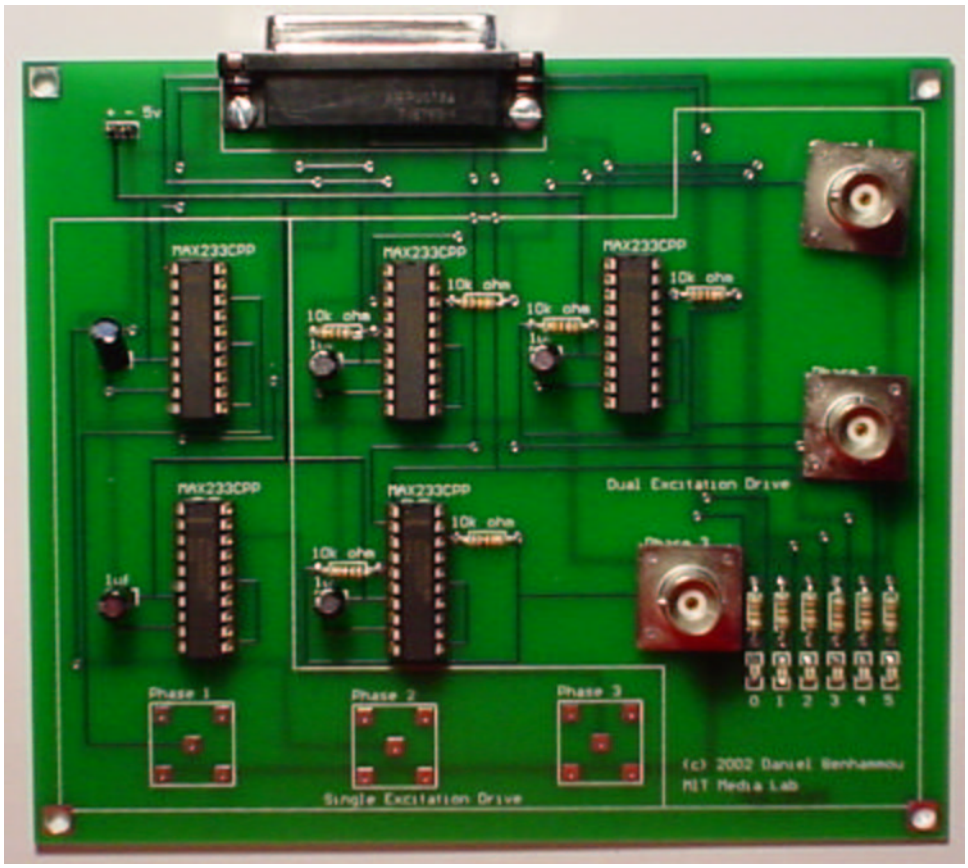

Figure 4-7: Electrostatic Driver Board

Designing a circuit to control the switching is relatively simple and just involves adding a few components on top of the circuitry used for the previous experiment. The new circuit uses one of the MAX233 ICs for each channel. Two bits from the parallel port were used as the inputs to the MAX233. The outputs, +10v, −10v and 0v were then connected through resistors to give the desired output. The board in figure 4-7 replaces the electronics for the single excitation drive (figure 3-7) and serves as the driver for the dual excitation electrostatic drive. LEDs have been added to visualize the output generated by the code in appendix A.2.

4.5 Software

The software needed to drive the DEMED is extremely similar to the code developed for the single excitation electrostatic drive. The only differences are that the code must be adjusted to support two bits per phase and the code repeats sequences of four bits as opposed to three. Table 4.3 shows the necessary outputs of the parallel port and the hex value needed

Table 4.3: Parallel Port Driver Chart

Bits								Hex
7	6	5	4	3	2	1	0	Value
∅	∅	1	0	1	1	1	0	0x2e
∅	∅	1	1	1	0	0	0	0x38
∅	∅	1	0	0	0	1	0	0x22
∅	∅	0	0	1	0	1	1	0x0b

to control the bits.

4.6 Prototype DEMED

The following section breaks down the prototype dual excitation multiphase electrostatic drive into all the components and describes how each was made.

4.6.1 Stator

The purpose of this experiment was to demonstrate large-scale electrostatic actuation on a low cost-scale. The experiment involved designing a printed circuit board containing an array of linear electrodes. The board was designed such that a three phase high voltage power supply would drive the device.

The performance of the electrostatic drive was limited for the most part by the stringent design specifications imposed by the company fabricating the printed circuit board. In order to achieve the goal of producing inexpensive, electrostatic motors, certain criteria had to be met. The printed circuit board was laid out as two layers on a ten inch square FR-4 board. All traces were deposited with 1 ounce copper plate and the traces were limited to six mil lines. All vias had a minimum diameter of 15 mils with a pad diameter of 25 mils. The minimum clearance for the board was 5 mils.

The stator is laid out on a ten inch by ten inch square of FR-4. The top layer of the board consists of 321 electrodes. Every third electrode is connected via 20 mil traces on the back side of the board. This layout conveniently allows for three phase voltage to generate the electrostatic potential. The board and traces are covered with a solder mask to prohibit electrostatic breakdown in the air between electrodes.

Around the perimeter of the board are 20 holes, each having a diameter of .130 inches. These hole were designed such that the stator could easily be mounted on a pressurized bed of gas to create an air bearing. In previous experiments, friction had proven to be one of the

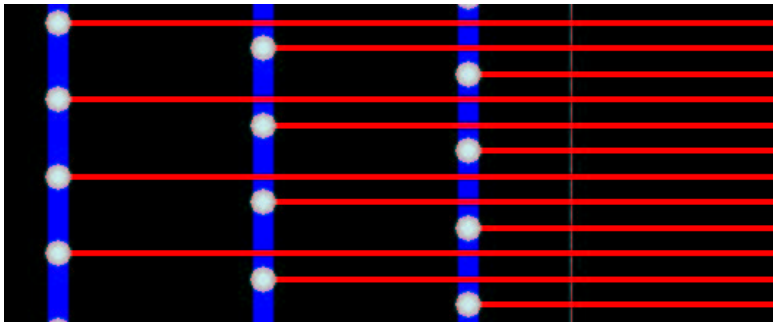

Figure 4-8: Trace spacing on FR-4 prototype board

most difficult obstacles to overcome [10]. To overcome this, at regular intervals across the board is a matrix of small holes, each having a diameter of 15 mils. The purpose of these holes is once the board is mounted on the pressurized table, the air passes through the holes reducing the friction.

We must derive an equation that lets us view the friction as a result of air pressure. To do this, we begin with Bernoulli's flow equation:

$$0 = \int_1^2 \frac{\partial V}{\partial t} ds + \frac{P_1 - P_2}{\rho} + \frac{\mathcal{V}_2^2 - \mathcal{V}_1^2}{2} + g(z_2 - z_1). \tag{4.14}$$

Since the flow is steady state, the partial differential term drops out. In addition, since the initial velocity of the gas, the difference in height and the exit pressure are all negligible, we can solve directly for the velocity of the gas flowing through the holes:

$$\mathcal{V}_2 = \sqrt{\frac{2P_1}{\rho}} \tag{4.15}$$

In order to determine the pressure loss through the holes, we had to first calculate the Reynolds number using $Re = \frac{\rho \mathcal{V} d}{\mu}$, which gives us a value of Re above the critical value [23]. Since the Reynolds number is above the transition value, we must assume that the flow is turbulent when using the following formula to calculate the head loss:

$$h_f = f \frac{L}{d} \frac{\mathcal{V}^2}{2g}. \tag{4.16}$$

To calculate the final pressure drop across the holes, we have to multiply equation 4.16 by the density ρ and substitute the velocity from equation 4.15. The result is the loss in pressure

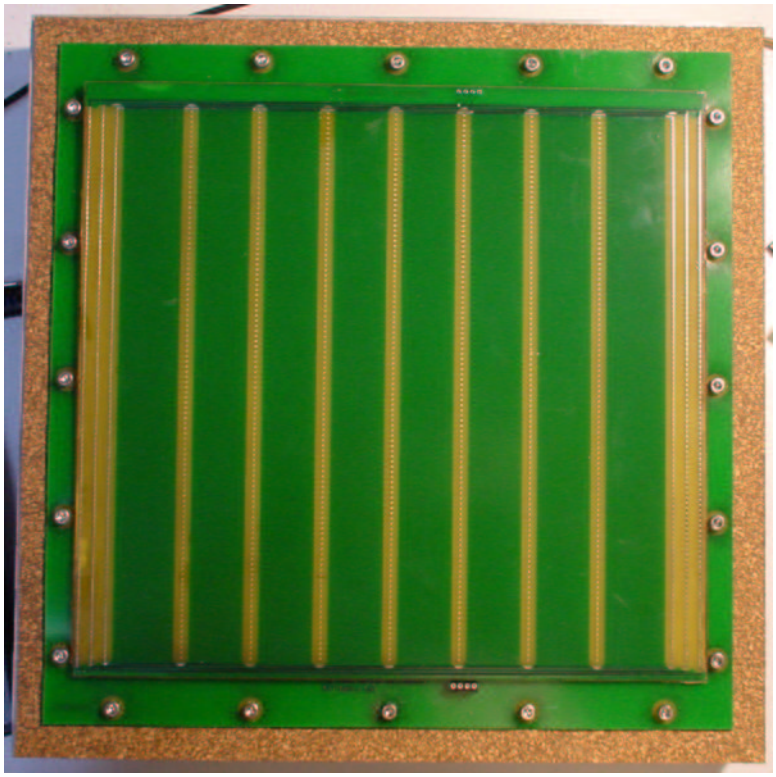

Figure 4-9: This figure shows the stator PCB mounted on the air table.

from the pressure reservoir in the air bed which is

$$\Delta P = \frac{fLP_1}{dg}. \tag{4.17}$$

To get the force from the compressed air that act on the slider, we must multiply the number of holes by the cross-sectional area of each hole to get the total area exposed to the air and then multiply by the pressure. We know that there are 200 holes with a diameter of 15 mils or 381 microns that gives a total area of 200 x 1.14e-7 square meters. By dividing the force by gravitational acceleration, it is possible to solve implicitly for the maximum mass that the air table can float:

$$M_{max} = \frac{AP_1}{g}\left(1 - \frac{fL}{dg}\right) \tag{4.18}$$

4.6.2 Slider

Due to the design of the hardware, multiple slider configurations could be tested using the same stator and air table. For the sake of simplicity, a slider was constructed out of one of the slightly modified stator boards. Once the board is received back from production, the

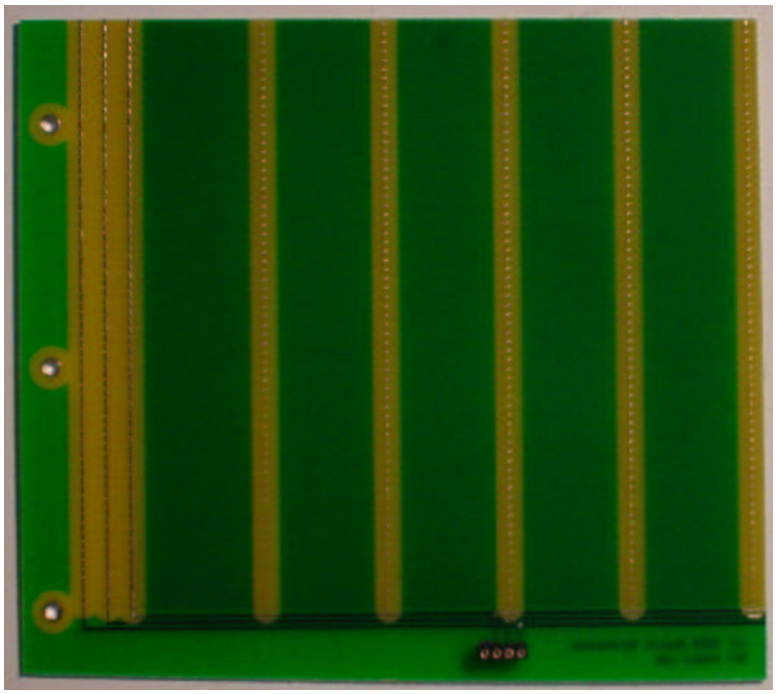

Figure 4-10: Slider for DEMED

board is trimmed using a high powered laser to insure a straight cut. The board is cut so that it fits snuggly with two Teflon rails mounted on the air table. The slider used in the experiments in the following section can be seen in figure 4-10.

In order to test the practicality of using easily fabricated electrostatic motors, one of the embedded electrode arrays created using the Roland vinyl cutter was used.

4.7 Experimental Results

With the hardware complete, experiments could be performed using the floater table and electronics. Due to complications with the electrode arrays fabricated on the Roland vinyl cutter, the electrodes on the printed circuit board were used as both the stator and the slider. Two sets of experiments were performed: the first used nitrogen in for floating the slider and the second used air. Figure 4-11 shows nitrogen connected for the gas bearing.

4.7.1 Nitrogen Bearings

The first set of experiments performed involved using nitrogen as the gas for the air bearing for the slider. One of the large cylinders of liquid nitrogen seen in figure 4-11 was connected to the air table and the valve was open to pressurize the reservoir to approximately five pounds

Figure 4-11: Liquid nitrogen cylinder used to test air bearing.

per square inch pressure. To test the functionality of the air bearing, a blank printed circuit board was placed on the stator board with the gas running. The test board floated nearly frictionless around the stator. In order to determine the coefficient of friction to calculate the minimum force require to move the slider when driven, the air table was inclined until the test PCB floated down. Since the coefficient of friction, μ is simply,

$$\mu = \tan\theta, \tag{4.19}$$

where θ is the angle at which sliding begins, μ was determined to be less than 0.01 since the test board started sliding when θ was less than one degree. The stator used in the experiments had a mass of 63.2 grams meaning that the minimum force require to move the slider would be $mg\mu$ or approximately 2.199 millinewtons.

The procedure for testing the electrostatic motor involved several steps. First, any modifications to the driving program were changed and then compiled. The program was then executed and tested using an osciloscope. Once the program was confirmed to be running, the slider was placed on the stator and connected to the output of the Trek voltage amplifiers. With the slider in place, the nitrogen valve was opened just enough to provide an adequate air bearing, but not so much that the stator board flexed under the pressure of the air reservoir. Finally, the voltage amplifiers were switched on and then observations could be made.

Upon switching on the voltage amplifiers for the first time, the smell of burning was

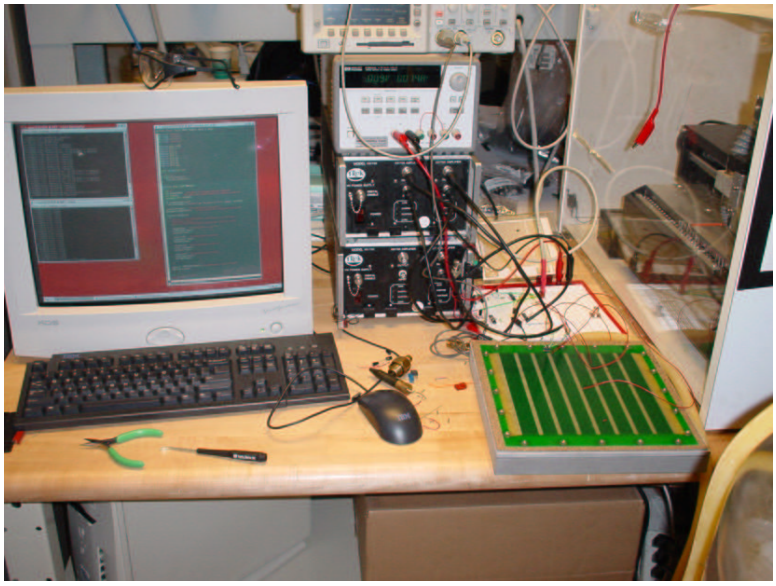

Figure 4-12: Stator and driving hardware prior to initial test.

immediately present as sparks danced across the entire board. Testing the output of the Trek 50/750 amplifiers with a digital multimeter showed that their peak output values were ±893 volts. This difference meant that at certain times, the electrodes carried a potential of 1786 volts. Examining the stator board closely revealed the real problem causing the dielectric breakdown of across the board: the cold nitrogen gas from the cylinder caused water vapor from the air to condense on the board causing short circuits. This showed that only compressed nitrogen could be used and not gas from a liquid nitrogen cylinder. Since no cylinders of compressed nitrogen were available, a line of compressed, dry air was brought over to serve as the air bearing.

4.7.2 Compressed Air Bearings

Compressed air works much better as an air bearing since it is not stored at a temperature of 77 degrees Kelvin. Using the same procedure as the nitrogen, the electrostatic drive was tested, this time using air as a bearing. Once again, the drive shorted out as the stator and slider lit up with sparks of dielectric breakdown. Examining the stator did not reveal any traces of condensation so an acrylic dielectric spray was applied to both the stator and the slider in several coats. The goal of this spray was to increase the dielectric breakdown distance so that the DEMED would not short out.

In an additional effort to stop the dielectric breakdown between electrodes on the stator, a signal attenuator was used to reduce the range of the inputs into the Trek voltage amplifier

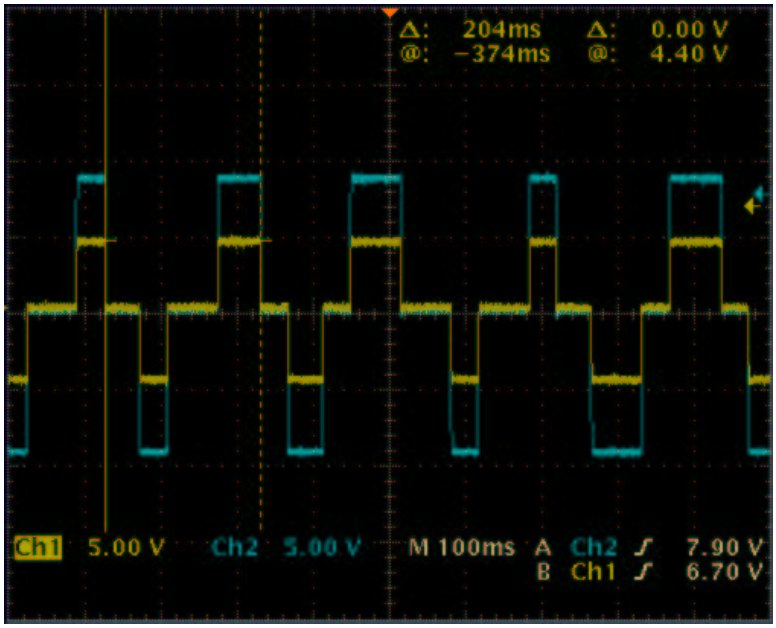

Figure 4-13: Osciloscope reading of output from MAX233 (blue) and attenuated signal (yellow).

(figure 4-13). The signal attenuator simply consisted of several resistors connected to ground which reduced the signal input to the voltage amplifiers to ±5 volts and the output to ±450 volts. The short circuits caused by the condensation on the stator caused carbonization between some of the electrodes in effect creating a resistor between phases of electrodes. This resistance canceled the effect of the multiphase drive so no motion was achieved without replacing the stator. After the stator was replaced, a new slider was cut and dielectric acrylic spray was applied to both components. Following the same procedure as before with the attenuated signal and new stator and slider produced the first successful experimental results.

The effect of lowering the driving voltage was surprisingly helpful. Upon turning on the voltage amplifiers, the slider immediately started moving chaotically. Part of the reason that the board did not simply move in the direction perpendicular to the electrodes was that the code does not initiate motion in either direction due to the configuration of the electrodes.

The first step in analyzing the movements of the slider was to take quantitative measurements and collect data. To collect data, a ruler was placed as one of the guiding rails for the slider, the other being Teflon due to its low friction. A video camera was then mounted on a tripod and focused on the DEMED. The voltage amplifiers were then switched on with a frequency of approximately five hertz (figure 4-13). The camera's video consists of individual

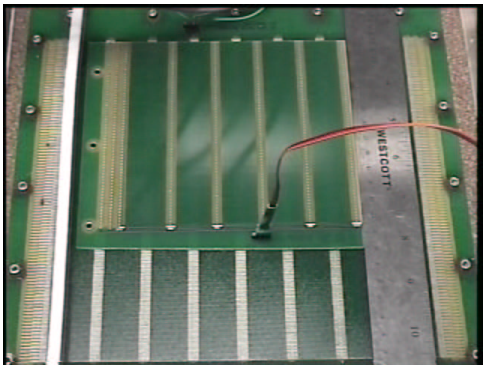

Figure 4-14: This figure shows the slider at time $T = 0$ seconds.

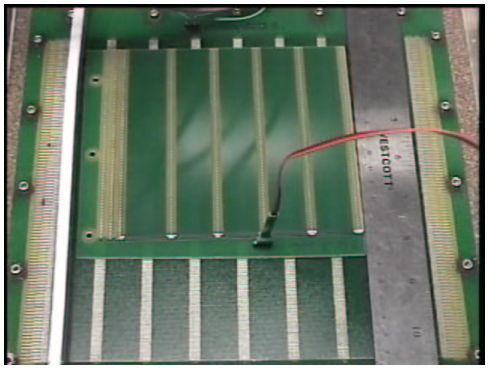

Figure 4-15: This figure shows the slider at time $T = 0.2667$ seconds.

frames at a rate of 30 hertz so data was collected with reasonable resolution. Figures 4-14 through 4-19 show still frames of the slider over the course of its 1.36 second journey.

The video was then transfered to there computer where it was digitized. A short segment where the slider traveled 2.5 centimeters in 1.4 seconds was selected and analyzed. Data was taken at every increment of five millimeters along its path. The result was six data points relating the displacement to the time. This displacement data can be seen in figure 4-20. Taking the data from figure 4-20, the plot was discretely differentiated to give data for the velocity of the slider as a function of time, figure 4-21. The same technique of discrete differentiation was done on the velocity to give the acceleration of the slider as a function of time: figure 4-22.

Examining figure 4-21 shows what we would expect from a DEMED. The slider accelerates at some rate from rest. The maximum velocity is coincident with the time when the velocity and the frequency compliment each other. This suggests that the most efficient way to drive and electrostatic motor would be to adjust the frequency depending on the velocity. This would mean that when the slider is at rest, the initial driving frequency starts very low and then as the velocity increases, the frequency of the driving signal also increases.

The maximum acceleration of -7cm/s^2 is also coincident with the time when the driving frequency matches the velocity. This peak in the acceleration also gives us the maximum driving force of the electrostatic motor since $F = ma$. Using the mass calculated earlier of 63.2 grams, we calculate the maximum force to be 0.004424 Newtons.

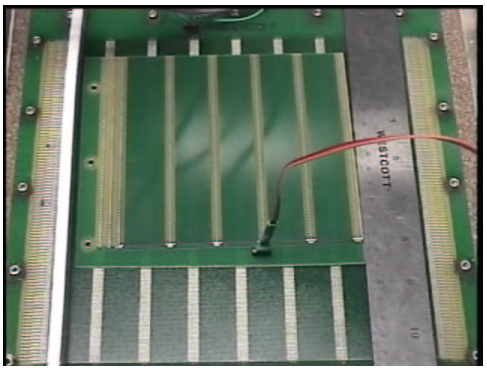

Figure 4-16: This figure shows the slider at time $T = 0.4333$ seconds.

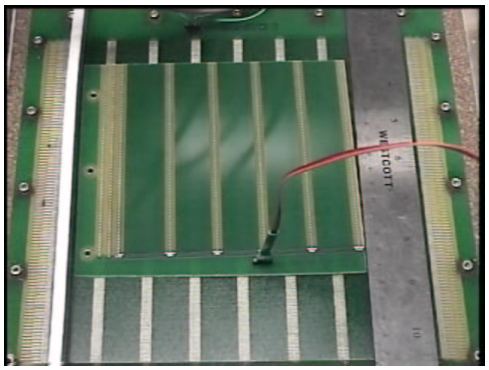

Figure 4-17: This figure shows the slider at time $T = 0.6667$ seconds.

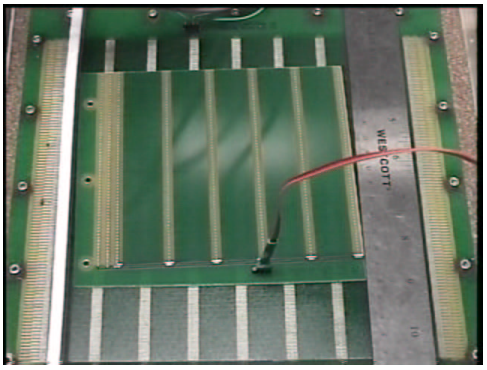

Figure 4-18: This figure shows the slider at time $T = 0.9667$ seconds.

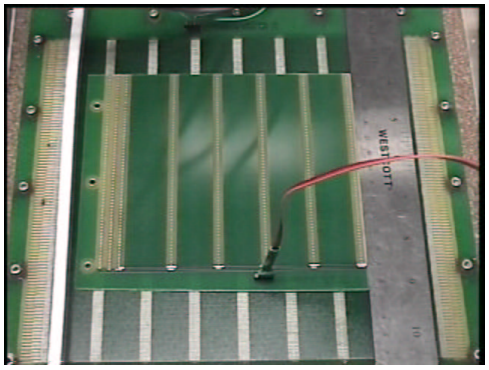

Figure 4-19: This figure shows the slider at time $T = 1.3667$ seconds.

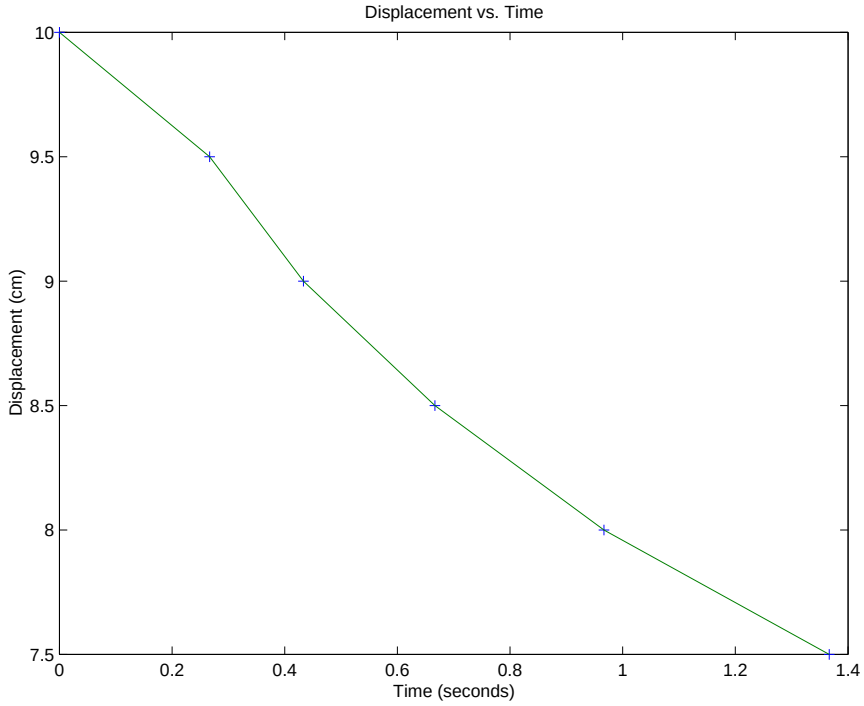

Figure 4-20: Displacement versus Time plot.

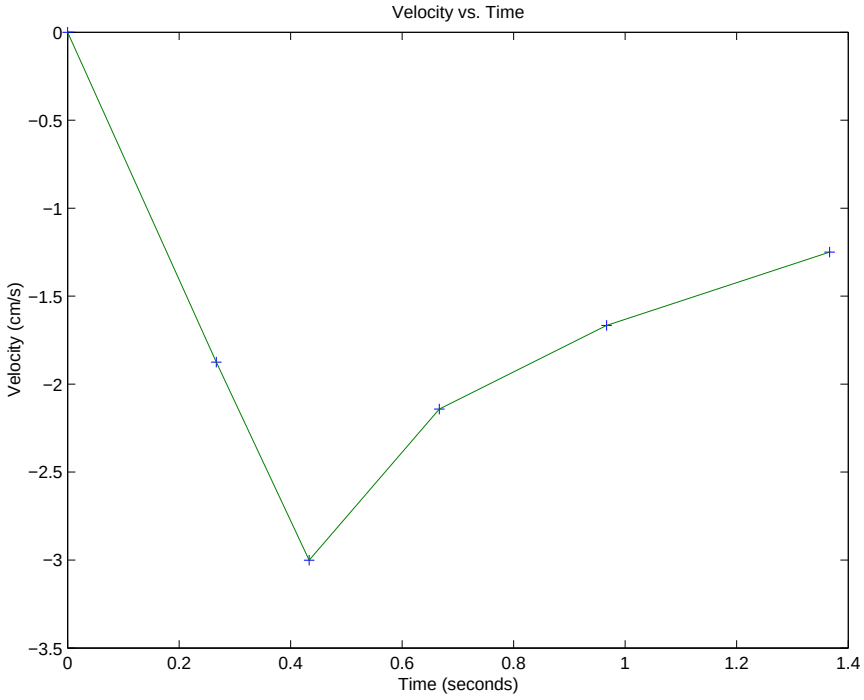

Figure 4-21: Velocity versus Time plot.

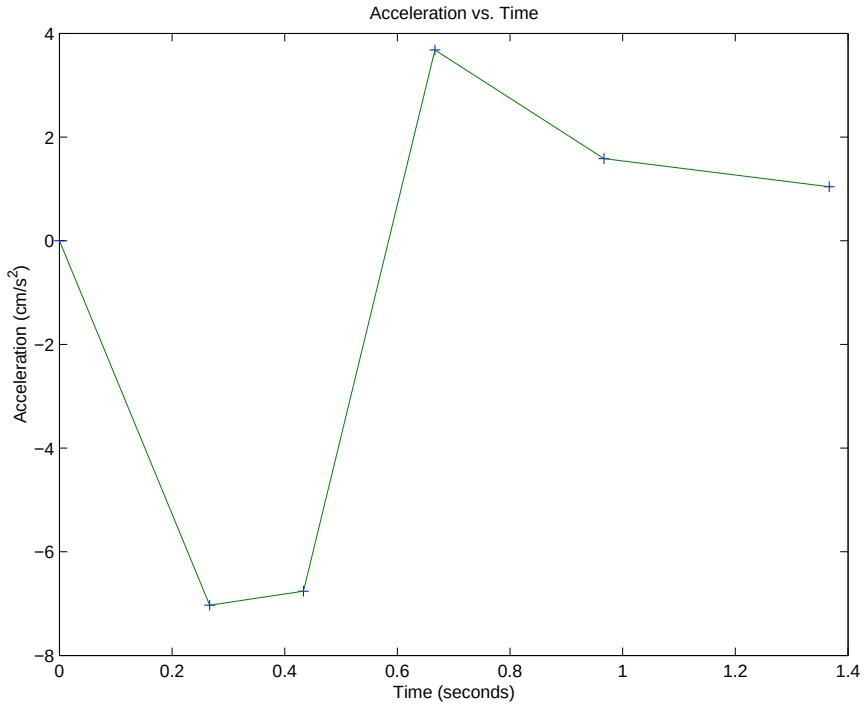

Figure 4-22: Acceleration versus Time plot.

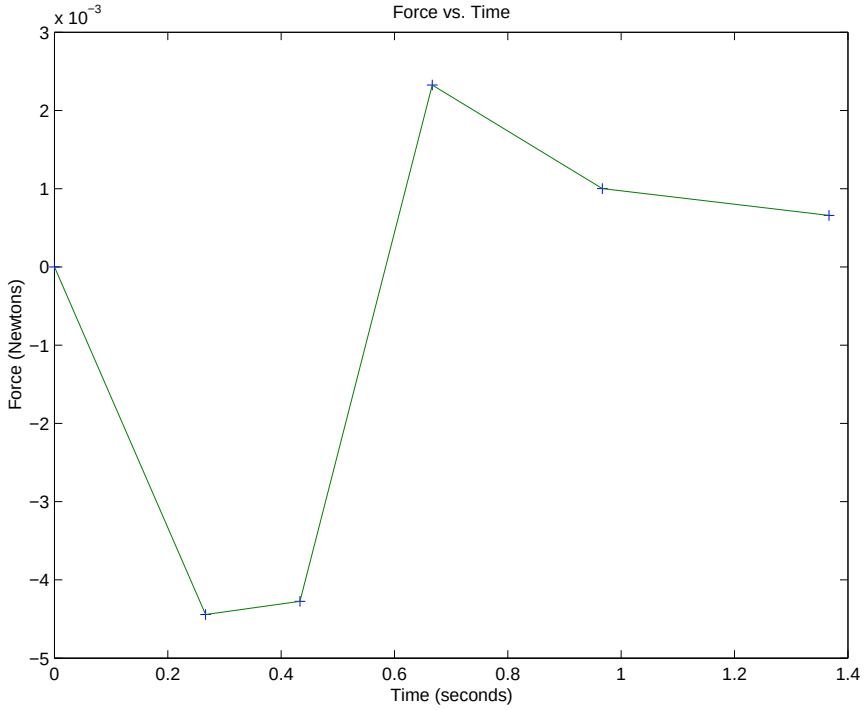

Figure 4-23: Force versus Time plot.

Chapter 5

Conclusions and Further Works

We have demonstrated in theory and showed in practice that macroscopic electrostatic motors are feasible. At the end of chapter three, we showed it was possible to use electrostatic forces to move a small piece of dielectric material by only driving one side. This was an important result because it showed that electrostatic forces are indeed strong enough to move objects, but we also learned that frequency and time were critical parameters.

The finite element analysis in chapter four predicted small forces acting on an electrostatic drive; however by using air bearings, we were able to all but eliminate friction so the main concern was getting the slider moving. It turns out that the two biggest difficulties that arose in the development, fabrication and actuation of the electrostatic drive was electrode fabrication and dielectric breakdown.

A substantial portion of chapter three was dedicated strictly to the development and fabrication of embedded electrode arrays. The two fabrication processes that offered the most flexibility and easiest path for iterations were the Roland vinyl cutter and the Universal Systems laser cutter. The vinyl cutter delivered the best results between the two fabrication machines; however it was also unreliable. The Roland had the capability to make fine cuts but the electrode width could not be less than roughly 35 mils. Problems also frequently arose due to the unpredictable sharpness of the knife, and the speed and pressure on the blade. Without the right combinations of values for each of these parameters, the vinyl cutter had mixed results. If the pressure was too hard, the speed to fast or if the cut was parallel to the direction of the roll, the electrodes had a tendency to peel off the wax sheet. Once the electrode array was cut, transferring the copper onto a substrate was non trivial. Often times stress in the copper from the cutting process would make the cut electrodes extremely susceptible to misalignment and they would frequently peel off. Once the right combination of parameters were established, designs could easily be laid out and cut - the

only bounds being the 35 mil trace width.

The Universal Systems laser cutter is one of the most versatile tools for electrode fabrication. The machine is extremely simple to use and very complicated designs can be produced. The main drawbacks are that the minimum cut width is several hundred microns but most of all, finding a material that is compatible with the laser cutter and still makes suitable electrodes is extremely challenging. We determined that with common materials, laser cutting an electrode mask was extremely difficult to fabricate. Laser-cutting conductive material is possible, however most conductive materials that can be cut with the laser cutter are reflective and as a result, have scalloped cuts with poor line definition.

Further work on the subject should perhaps focus on special conductive inks. The conductive ink described in chapter three was an excellent conductor, but much too viscous to use as a printable ink. Current printing technology would allow for extremely fine resolution if an ink could be developed with conductive properties. Possibilities include saturating an ink solution with extremely fine carbon powder. Since very little charge is flowing, high resistance is an acceptable characteristic for an electrostatic motor. In addition, if conductive solutions could be used in normal ink jet printers, then the price of electrode fabrication would be extremely low.

Perhaps the biggest obstacle uncovered in this research was dielectric breakdown. Nearly all of the work done in the past on electrostatic motors have used a dielectric fluid to prevent breakdown [25, 26, 16, 15]. Since the dielectric breakdown in air is 1000 volts per millimeter and the motors designed in this thesis often worked in closer proximity, dielectric breakdown was imminent. Part of the reason that this occurred so frequently was also partially due to the fact that the solder mask did not cover the vias in the stator board. This meant that the electrodes around all the holes on the stator were open to air and in many cases, the clearance is very close to a millimeter.

Not only does dielectric breakdown between electrodes ruin the board, it can also be dangerous. Using a dielectric fluid has the added benefit that it acts as lubrication as well as insulation, but significantly reduces the number of applications for which electrostatics would be otherwise useful. Further directions for this could include trying to use an intermittent layer between the stator and the slider that has very low friction and a high dielectric constant. As the experiment showed, however, the force produced by the electrostatic forces was extremely small and without using the air bearing, movement would not have been possible. Therefore, it is also important as a direction of future development that the material in between the electrodes have an extremely low coefficient of friction. In addition, prior works have shown that the output force on the slider increases almost exponentially as the

potential driving the motor is increased. If a better dielectric was used in between the stator and the slider, it would be possible to increase the voltage, leading to higher force output.

The peak force observed in the experiments at the end of chapter four suggest that electrostatic drives may be extremely weak. The motor used in the experiment was only strong enough to accelerate the board 0.07m/s^2 with 4.424 millinewtons. Further development of macroscopic actuation must determine if the performance can be improved. Using the easily fabricated electrodes, the performance does not suggest that a motor driven by electrostatic forces would do much of anything if loaded. Some of the work on MEMS scale electrostatic actuation have focused on stacking the arrays of electrodes and found that the force scales linearly with the number of electrodes [26]. This is not surprising because this problem is really about optimization. The more electrodes added, the more force the motor will produce, but it will also weigh more. At a certain point, the slider would be completely overcome by the weight of the electrodes and would not slide regardless of the thrust force since the forces are always attractive and the boards would get stuck together.

The experiments also showed that as the speed of the electrostatic motor approached the driving frequency, the motor hit its peak velocity and force (figures 4-21 and 4-22). This suggests that if the frequency starts slow and ramps up as the velocity increases it would be possible to stay on the leading edge of the force and keep accelerating the slider. This optimization control would be most effectively implemented by means of a closed feedback loop [21]. Perhaps the easiest way to actively sense the location of the slider in relation to the stator would be to add another trace to the slider. This trace would not be driven, but it would sense the capacitance in relation to the stator electrodes. The signal from the sensor trace could then be fed in a microprocessor to determine the phase and the position of the slider. By doing this, the microprocessor could then control the driving frequency to optimize the driving system and increase the velocity and force of the motor [21].

In conclusion, we saw that large-scale electrostatic actuation is possible and can be produced affordably. Many challenges stand in the way of having table surfaces that move or walls that slide under electrostatic force. Hopefully further development in this area of motors will lead to a revolution in actuation.

Appendix A

Source Code

A.1 Single Excitation Driver

```
#include <stdio.h>
#include <stdlib.h>
#include <unistd.h>
#include <asm/io.h>

#define base 0x378
#define BIT0 1
#define BIT1 2
#define BIT2 4
#define BIT3 8
#define BIT4 16
#define BIT5 32
#define BIT6 64
#define BIT7 128

void dusleep(int num)
{
  int i,j;
  for(j=0;j<num;j++)
    for(i=0;i<1000;i++);
}

main(int argc, char **argv)
{
  int i;
  int freq=16000;   /* number of microseconds per phase */
  int time=1;      /* number of seconds times 5 to charge slider */
  unsigned char value=0;
```

```
30
    if (ioperm(base,1,1))
      fprintf(stderr, "Couldn't get the port at %x\n", base), exit(1);

    outb(0x05,base);     /* 1 second per million */
    dusleep(time*1000000);   /* sets charge for single excitation */

    for(i=0;i<500;i++)
      {
        /* value |= BIT0|BIT1|BIT2;  setting bit 0,1,2 as high
        outb(value, base);                                          40
        value &= ~(BIT0|BIT1|BIT2); setting bit 0,2,3 as low */

        value=0x06;   /* setting bits to 110 */
        outb(value, base);
        dusleep(freq);

        value=0x05;   /* setting bits to 101 */
        outb(value, base);
        dusleep(freq);
                                                                    50
        value=0x03;   /* setting bits to 011 */
        outb(value,base);
        dusleep(freq);
      }

    value &= ~(BIT0|BIT1|BIT2); /* setting bit 0,2,3 as low */
    outb(value,base);
  }
```

[20]

A.2 DEMED Driver

```
#include <stdio.h>
#include <stdlib.h>
#include <unistd.h>
#include <asm/io.h>

#define base 0x378
#define BIT0 1
#define BIT1 2
#define BIT2 4                                                      10
```

```
#define BIT3 8
#define BIT4 16
#define BIT5 32
#define BIT6 64
#define BIT7 128

void dusleep(int num)
{
  int i,j;
  for(j=0;j<num;j++)                                                    20
    for(i=0;i<1000;i++);
}

main(int argc, char **argv)
{
  int i;
  int freq=16000;    /* number of microseconds per phase */
  int time=1;      /* number of seconds times 5 to charge slider */
  unsigned char value=0;
                                                                        30
  if (ioperm(base,1,1))
    fprintf(stderr, "Couldn't get the port at %x\n", base), exit(1);

  outb(0x05,base);     /* 1 second per million */
  dusleep(time*1000000);    /* sets charge for single excitation */

  for(i=0;i<500;i++)
    {
      /* value |= BIT0|BIT1|BIT2;  setting bit 0,1,2 as high
      outb(value, base);                                                40
      value &= ~(BIT0|BIT1|BIT2); setting bit 0,2,3 as low */

      value=0x2e;    /* setting bits to 101110 */
      outb(value, base);
      dusleep(freq);

      value=0x38;    /* setting bits to 111000 */
      outb(value, base);
      dusleep(freq);
                                                                        50
      value=0x22;    /* setting bits to 100010 */
      outb(value,base);
      dusleep(freq);

      value=0x0b;    /* setting bits to 001011 */
```

```
        outb(value,base);
        dusleep(freq);

      }

  value &= ~(BIT0|BIT1|BIT2); /* setting bit 0,2,3 as low */
  outb(value,base);
}
```

Appendix B

Physical Properties of Gases

Table B.1: Properties of Air

Property	Symbol	Value	Units
Density	ρ	1.2033	kg/m^3
Viscosity	μ	1.80×10^{-5}	$N \cdot s/m^2$
Universal Constant	R	287	$m^2/(s^2 \cdot K)$

Table B.2: Properties of Nitrogen

Property	Symbol	Value	Units
Density	ρ	1.1625	kg/m^3
Viscosity	μ	1.76×10^{-5}	$N \cdot s/m^2$
Universal Constant	R	297	$m^2/(s^2 \cdot K)$

Appendix C

Ansys Scripts

C.1 Modeling Electrodes

```
/batch,list
/show,combp,grph]
/title, Comb Drive Example
/prep7
! dimensions (microns) / parameters
wf=2                    ! Fixed  finger width
wm=2                    ! Moving finger width
gg=2                    ! Gap
tt=40                   ! Moving length
t1=4                    ! Fixed finger backing
t2=tt                   ! Moving finger length
hh=10                   ! Height
dt=tt/2
V0=10
xx=(2*tt-dt)*2.75
y1=(wm/2)+gg
y2=(wm/2)+gg+wf
x1=tt+t1
! Create Model
cyl4,0,0,xx,0,,360,1
! ----- Syntax: CYL4,xcenter,ycenter,innerrad,startang,[outerrad],endang,depth
! ----- What we have is a very thin ~(1:165) cylinder
block,-tt,0,y1,y2,0,1
! ----- Syntax: BLOCK,x1,x2,y1,y2,z1,z2
block,(-tt-t1),-tt,-y2,y2,0,1
! ----- Note: Blocks take up the entire thickness of cylinder
block,-tt,0,-y1,-y2,0,1
block,-dt,(tt-dt),(-wm/2),(wm/2),0,1
block,(-dt-(gg/2)),(tt-dt+(gg/2)),((-wm/2)-(gg/2)),(wm/2)+(gg/2),0,1
dx=wm*1.1
dy=dx
block,-x1-dx,tt-ddt+dx,-y2-dy,y2+dy,0,1
vovlap,all
```

```
! ----- "Overlaps" all volumes; partitions selected (in this case, all)
 volumes according to their intersections
/com  ---------------------------------------
/com  Volume  Component
/com  ---------------------------------------
/com  2,8,9   Fixed Finger
/com   5      Moving Finger
/com   11     Air Layer around Moving Finger
/com   12     Air Layer around the Comb Drive
/com   10     Boundary <---- cylinder minus interesting parts
/com  ---------------------------------------
! 2D mesh
et,11,200,7              ! Use high order tri mesh element
! ----- Syntax: ET,<integer label you want to refer to type by>,ElemName,
<options...>
esize,gg/2
! ----- Syntax: ESIZE,SIZE --- sets default size of element edge on boundaries
mshap,1                  ! Force a traingle mesh
! ----- Syntax: MSHAPE, KEY <-- sets triangle mesh
amesh,52                 ! Mesh air layer around moving finger
! ----- Mesh area #52, apparently using current element type
esize,gg
amesh,54                 ! Mesh air layer around comb drive
esize,(y2+dy)*5
amesh,50                 ! Mesh boundary

! ----- Up to this point we were only meshing front plane/face of cylinder

! 3D mesh
et,1,128
emunit,epzro,8.854e-6    ! Free space permittivity (uMKSV units)
mp,perx,1,1              ! Set relative permitivity to 1
! ----- Syntax: MP,<MaterialPropertyLabel>,<Material#Label>
mat,1
! ----- MAT, <Material#Label>;   sets material for all following elements
lsel,s,loc,z,.5
! ----- select all lines whose z-center is 0.5 (effectively,
lines along cylinder length)
lesize,all,,,1           ! Set element size in z-direction to 1
! ----- change number of element divisions on unmeshed lines to 1
lsel,all
! ----- select all lines
type,1
! ----- switch back to element labeled 1 (volume elt)
vsel,s,volu,,10,12,1
! ----- select volumes 10 through 12; everything except the metals
vsweep,all               ! Create wedge volume elements from tri mesh
! ******* project tri mesh into 3-D mesh !!!!!!!!!!!!!!!!!!!!!!!!!!!!
vsel,all
vsel,s,volu,,10          ! Plot model !-- select boundary volume
eslv,s
```

```
! Select the elements that are part of the selected volumes (all elements, I think)
eplot
! Equivalent to UtilityMenu:Plot:Elements
allsel
! Select everything
asel,s,loc,z,1          ! Select original areas
! ----- because only original areas have an average z-component of 1
aclear,all
! ----- delete all the selected areas and the nodes in those areas
etdele,11               ! Remove meshing elements
! ---- what we have done is: 1) mesh one face of the world,
2) project that mesh into 3-D; 3) delete the original ! ---- mesh.
asel,all
csys,1
! ----- activate coordinate system #1 (cylindrical)
nsel,s,loc,x,xx
! ----- now that we are in cylindrical coords,
select all the nodes on the outer boundary
d,all,VOLT,0            ! Apply volt=0 at outer boundary
! ----- Syntax: D,<node# or all>,<DOF label>,<value>
nsel,all
csys,0
! --- switch back to Cartesian coordinates
vsel,s,volu,,5
! --- select volume #5
cm,MFINGER,volu
! --- group selected volumes (#5, the finger vol) into a component called MFINGER
asel,s,ext
! --- select areas on the exterior (surface?) of the selected volume
nsla,s,1
! --- select all nodes on the selected areas, in this case:
surface air elt of moving finger
d,all,VOLT,0            ! Apply a zero potential on the moving finger
sf,all,mxwf
!--- label all of these nodes with "surface loads" -- Maxwell Force flags,
 so the force on them will be calculated
vsel,s,volu,,2
vsel,a,volu,,8,9,1
cm,FFINGER,volu
asel,s,ext
nsla,s,1
d,all,VOLT,V0           ! Apply 10 Volts on the fixed finger
allsel
! p-convergence control
pemopt,5.0,dual         ! Select Dual Method with tolerance of 5%
! --- Use dual when working with >1 dielectric material
pconv,2,efor,x          ! Base convergence on Maxwell forces with tolerance of 2%
! --- Sets convergence values; Syntax: PCONV, Tolerance,
(Global ES force), (x-component)
/gst,on
! --- Turn graphical solution tracking on
```

```
save
! --- SAVE_DB
finish
! --- Exit preprocessor
/solu
eqslv,iccg               ! Set iccg solver
solve
finish
/post1
set,last                 ! Set the last data step
! --- Select most recent data set for postprocessing
vsel,s,volu,,11,12
eslv,s
pplot                    ! Plot the p-levels around the fingers
esel,all
plconv,all               ! Plot the convergence curve
etable,fx,fmag,x
!-- create a table called fx that contains the "x" component of
"fmag" for every elt
etable,fy,fmag,y
etable,fz,fmag,z
ssum
!--- calculate and print the sum of element table items
*get,fx,ssum,,item,fx    ! Get summed forces
*get,fy,ssum,,item,fy
*get,fy,ssum,,item,fz
/com,Comb Drive Force
*stat,fx
finish
```

[24]

C.2 Modeling Parameters

```
/BATCH
! /COM,ANSYS RELEASE  5.6.2  UP20000525       15:47:33    01/09/2001
!*
/FILNAME,esmotor1,0
/PREP7
!*
/NOPR
/PMETH,OFF,1
KEYW,PR_SET,1
KEYW,PR_STRUC,0
KEYW,PR_THERM,0
KEYW,PR_FLUID,0
KEYW,PR_ELMAG,1
KEYW,MAGNOD,0
KEYW,MAGEDG,0
KEYW,MAGHFE,0
KEYW,MAGELC,1
KEYW,PR_MULTI,0
```

```
KEYW,PR_CFD,0
/GO
!*
! /COM,
! /COM,Preferences for GUI filtering have been set to display:
! /COM,  Electric
!*
! LGWRITE,esmotor1,lgw,c:\WINDOWS\Desktop\alexwg\ansys\,COMMENT
RECTNG,0,250e-6,0,1e-3,
RECTNG,0.00025,0.00050,0,0.001,
RECTNG,0.00050,0.00075,0,0.001,
RECTNG,0.00075,0.001,0,0.001,
RECTNG,0.001,0.00125,0,0.001,
! /PNUM,KP,0
! /PNUM,LINE,0
! /PNUM,AREA,1
! /PNUM,VOLU,0
! /PNUM,NODE,0
! /PNUM,TABN,0
! /PNUM,SVAL,0
! /NUMBER,0
!*
! /PNUM,ELEM,0
! /REPLOT
!*
! /PNUM,KP,0
! /PNUM,LINE,0
! /PNUM,AREA,1
! /PNUM,VOLU,0
! /PNUM,NODE,0
! /PNUM,TABN,0
! /PNUM,SVAL,0
! /NUMBER,0
!*
! /PNUM,ELEM,0
! /REPLOT
!*
RECTNG,0,0.00125,.001+12e-6,0.002+12e-6,
ADELE,       6
RECTNG,0,0.00125,.001+12e-6,0.0001+12e-6,
ADELE,       6
! /DIST, 1 ,0.729000,1
! /REP,FAST
! /DIST, 1 ,0.729000,1
! /REP,FAST
! /DIST, 1 ,1.371742,1
! /REP,FAST
! /DIST, 1 ,1.371742,1
! /REP,FAST
RECTNG,0,0.00125,.001+12e-6,0.0011+12e-6,
! /DIST, 1 ,0.729000,1
```

```
! /REP,FAST
! /DIST, 1 ,0.729000,1
! /REP,FAST
FLST,3,1,5,ORDE,1
FITEM,3,1
FLST,2,5,5,ORDE,2
FITEM,2,1
FITEM,2,-5
ADELE,P51X
! SAVE, esmotor1,db,
! LGWRITE,esmotor1,lgw,c:\WINDOWS\Desktop\alexwg\ansys\,COMMENT
RECTNG,0,0.00025,0,0.0001,
RECTNG,0.00025,0.00050,0,0.0001,
RECTNG,0.00050,0.00075,0,0.0001,
RECTNG,0.00075,0.001,0,0.0001,
RECTNG,0.001,0.00125,0,0.0001,
ADELE,       6
RECTNG,0.001,0.00125,0.0001+12e-6,0.0002+12e-6,
RECTNG,0,0.00125,0.0001+12e-6,0.0002+12e-6,
ADELE,       6
! /DIST, 1 ,1.371742,1
! /REP,FAST
! /DIST, 1 ,0.729000,1
! /REP,FAST
! /DIST, 1 ,0.729000,1
! /REP,FAST
! /DIST, 1 ,1.371742,1
! /REP,FAST
! SAVE, esmotor1,db,
! SAVE, esmotor1,db,
! /PNUM,KP,0
! /PNUM,LINE,0
! /PNUM,AREA,0
! /PNUM,VOLU,0
! /PNUM,NODE,0
! /PNUM,TABN,0
! /PNUM,SVAL,0
! /NUMBER,0
!*
! /PNUM,ELEM,0
! /REPLOT
!*
! /PNUM,KP,0
! /PNUM,LINE,0
! /PNUM,AREA,1
! /PNUM,VOLU,0
! /PNUM,NODE,0
! /PNUM,TABN,0
! /PNUM,SVAL,0
! /NUMBER,0
!*
```

```
! /PNUM,ELEM,0
! /REPLOT
!*
! /PNUM,KP,0
! /PNUM,LINE,0
! /PNUM,AREA,1
! /PNUM,VOLU,0
! /PNUM,NODE,0
! /PNUM,TABN,0
! /PNUM,SVAL,0
! /NUMBER,0
!*
! /PNUM,ELEM,0
! /REPLOT
!*
!*
/TITLE,Electrostatic Motor 1
/UNITS, SI
/UNITS, SI
! SAVE, esmotor1,db,
!*
ET,1,PLANE121
!*
KEYOPT,1,3,0
KEYOPT,1,4,0
KEYOPT,1,5,0
KEYOPT,1,7,0
!*
!*
/NOPR
/PMETH,OFF,1
KEYW,PR_SET,1
KEYW,PR_STRUC,1
KEYW,PR_THERM,0
KEYW,PR_FLUID,0
KEYW,PR_ELMAG,1
KEYW,MAGNOD,0
KEYW,MAGEDG,0
KEYW,MAGHFE,0
KEYW,MAGELC,1
KEYW,PR_MULTI,1
KEYW,PR_CFD,0
/GO
!*
! /COM,
! /COM,Preferences for GUI filtering have been set to display:
! /COM,  Structural
! /COM,  Electric
!*
!*
ET,2,PLANE13
```

```
!*
KEYOPT,2,1,7
KEYOPT,2,2,0
KEYOPT,2,3,0
KEYOPT,2,4,0
KEYOPT,2,5,0
!*
!*
UIMP,1,EX, , , ,
UIMP,1,NUXY, , , ,
UIMP,1,ALPX, , , ,
UIMP,1,REFT, , , ,
UIMP,1,MU, , , ,
UIMP,1,DAMP, , , ,
UIMP,1,DENS, , , ,
UIMP,1,MURX, , , ,
UIMP,1,MGXX, , , ,
UIMP,1,RSVX, , ,1e14,
UIMP,1,PERX, , , ,
!*
!*
UIMP,1,EX, , , ,
UIMP,1,NUXY, , , ,
UIMP,1,ALPX, , , ,
UIMP,1,REFT, , , ,
UIMP,1,MU, , , ,
UIMP,1,DAMP, , , ,
UIMP,1,DENS, , , ,
UIMP,1,MURX, , , ,
UIMP,1,MGXX, , , ,
UIMP,1,RSVX, , , ,
UIMP,1,PERX, , , ,
!*
!*
UIMP,1,EX, , , ,
UIMP,1,NUXY, , , ,
UIMP,1,ALPX, , , ,
UIMP,1,REFT, , , ,
UIMP,1,MU, , , ,
UIMP,1,DAMP, , , ,
UIMP,1,DENS, , , ,
UIMP,1,MURX, , , ,
UIMP,1,MGXX, , , ,
UIMP,1,RSVX, , , ,
UIMP,1,PERX, , , ,
!*
!*
UIMP,2,EX, , , ,
UIMP,2,NUXY, , , ,
UIMP,2,ALPX, , , ,
UIMP,2,REFT, , , ,
```

```
UIMP,2,MU, , , ,
UIMP,2,DAMP, , , ,
UIMP,2,DENS, , , ,
UIMP,2,MURX, , , ,
UIMP,2,MGXX, , , ,
UIMP,2,RSVX, , ,1e14,
UIMP,2,PERX, , , ,
!*
!*
! SAVE, esmotor1,db,
! SAVE, esmotor1,db,
! LGWRITE,esmotor1,lgw,c:\WINDOWS\Desktop\alexwg\ansys\,COMMENT
```

[24]

C.3 Python Script

```
### Don't center any rects on (0,0)

fname = 'c:\\esm2.ans'
# plate = [[-2.0,-2.0,-0.5,-1.,5.],[0.5,1.,2.,2.,-5.]] # es plates
plate = [[-1.0,-2.0,1.,-1.,5.],[-1.,1.,1.,2.,-5.]] # es plates
thickness = 1.0

plate = []
origx = -2.0
origy = 0.0
pitch = 1.0
interpitch = pitch/2
depth = pitch/2
dist = pitch*2
for i in range(2):
plate.append([origx+i*(pitch+interpitch),origy-(dist+depth),
        origx+i*(pitch+interpitch)+pitch,origy-dist,((i%3)-1)*5])
plate.append([origx+(i+0.5)*(pitch+interpitch),origy+dist,
        origx+(i+0.5)*(pitch+interpitch)+pitch,origy+dist+depth,
(((4-i)%3)-1)*5])


universe_width = 50
boundrect = [-5,-5,5,5]
eltsize = 0.2

### NOTE: Use sel commands to get proper mesh areas
### Can still keep most of it

f = open(fname,"w")
f.write("""/title, Electrostatic Motor\n
/prep7\n""")

# create large flat cylindrical background
# f.write("cyl4,0,0,%f,0,,360,%f\n"%(universe_width,thickness))
```

```
for r in plate:
f.write("block,%f,%f,%f,%f,%f,%f\n"%(r[0],r[2],r[1],r[3],0,thickness))
f.write("block,%f,%f,%f,%f,%lf,%lf\n"%(boundrect[0],boundrect[2],
boundrect[1],boundrect[3],0,thickness))
f.write("vovlap,all\n")
f.write("vglue,all\n")

f.write("et,11,200,7\n")
#f.write("esize,%f\n"%(eltsize,))
f.write("asel,s,loc,z,1\n")
f.write("asel,r,loc,x,0\n")
f.write("asel,r,loc,y,0\n") # select BOTH boundrect and cyl face
f.write("mshap,1\n")
f.write("amesh,all\n");
f.write("asel,all\n");

### Begin the 3-D meshing

f.write("et,1,128\n");
f.write("mp,perx,1,1\n");
f.write("mat,1\n");
f.write("lsel,s,loc,z,%f\n"%(thickness/2,))
f.write("lesize,all,,,%f\n"%(thickness,))
f.write("lsel,all\n");
f.write("type,1\n");

f.write("vsel,s,loc,x,0\n")
f.write("vsel,r,loc,y,0\n") # select all non-metal volumes
f.write("vsweep,all\n")

# Remove original areas
f.write("asel,s,loc,z,%f\n"%(thickness,));
f.write("""aclear,all\n
etdele,11\n
asel,all\n""");
f.write("nsel,s,loc,x,%f\n"%(boundrect[0],));
f.write("nsel,a,loc,x,%f\n"%(boundrect[2],));
f.write("nsel,a,loc,y,%f\n"%(boundrect[1],));
f.write("nsel,a,loc,y,%f\n"%(boundrect[3],));
f.write("""d,all,VOLT,0\n
nsel,all\n
csys,0\n""");

# Now, work with the metals
#f.write("""vsel,all\n
#vsel,s,loc,x,0\n
#vsel,r,loc,y,0\n
#vsel,inve\n""")
for elec in plate:
f.write("vsel,all\n")
f.write("vsel,s,loc,x,%f\n"%((elec[0]+elec[2])/2,))
```

```
f.write("vsel,r,loc,y,%f\n"%((elec[1]+elec[3])/2,))
f.write("cm,ELEC%d,volu\n"%(plate.index(elec),))
f.write("asel,s,ext\n")
f.write("nsla,s,1\n")
f.write("d,all,VOLT,%f\n"%(elec[4],))
f.write("sf,all,mxwf\n");
f.write("""allsel\n
pemopt,5.0,dual\n
pconv,2,efor,x\n
/gst,on\n
save\n
finish\n
/solu\n
eqslv,iccg\n
solve\n
finish\n
/post1\n
set,last\n""")

f.write("vsel,s,loc,x,0\n")
f.write("vsel,r,loc,y,0\n")
f.write("""eslv,s\n
pplot\n
esel,all\n
plconv,all\n
etable,fx,fmag,x\n
etable,fy,fmag,y\n
etable,fz,fmag,z\n
ssum\n
*get,fx,ssum,,item,fx\n
*get,fy,ssum,,item,fy\n
*get,fy,ssum,,item,fz\n
*stat,fx\n
*stat,fy\n
*stat,fz\n
finish\n""")



f.close()
```

[24]

Appendix D

MATLAB Scripts

D.1 Data Plots

```
global displacement time velocity

displacement=10:-0.5:7.5;
time=[0,0.2667,0.4333,0.6667,0.9667,1.3667];

plot(time,displacement,'+',time,displacement,'-')
title('Displacement vs. Time')
ylabel('Displacement (cm)')
xlabel('Time (seconds)')

pause

i=size(time);
for I=2:i(2)
    velocity(1)=0;
    velocity(I)=(displacement(I)-displacement(I-1))/(time(I)-time(I-1));
end

plot(time,velocity,'+',time,velocity,'-')
title('Velocity vs. Time')
ylabel('Velocity (cm/s)')
xlabel('Time (seconds)')

pause

for I=2:i(2)
    acceleration(1)=0;
    acceleration(I)=(velocity(I)-velocity(I-1))/(time(I)-time(I-1));
```

```
end

plot(time,acceleration,'+',time,acceleration,'-')
title('Acceleration vs. Time')
ylabel('Acceleration (cm/s^2)')
xlabel('Time (seconds)')

pause

force=0.000632 .* acceleration;
plot(time,force,'+',time,force,'-')
title('Force vs. Time')
ylabel('Force (Newtons)')
xlabel('Time (seconds)')
```

Bibliography

[1] H. Anderson Ed. *A Physicist's Desk Reference* 2nd. Ed. American Institute of Physics, 1989.

[2] M. Ashby. *Engineering Materials 1*, 2nd Ed. Butterworth Heinemann, 1996.

[3] L. Bloomfield. "How Things Work: Electric Motors," http://howthingswork.virgia.edu 2001.

[4] K.-F. Böhringer *et al.* "Upper and lower bounds for progrmmable vector fields with applications to MEMS and vibratory plate parts feeders," International Workshop on Algorithmic Foundations of Robotics. 1996.

[5] K.-F. Böhringer *et al.* "Vector Fields for Task-level Distributed Manipulation: Experiments with Organic Micro Actuator Arrays," International Conference on Robotics and Automation. 1997.

[6] C. Brown. *Mini Motor Formed by Shape-Memory Alloy*, EE Times. 2001.

[7] B. Donald, Robotics Lab, Dept. of Computer Science, Stanford University.

[8] N. Gershenfeld. *The Physics of Information Technology*, Cambridge University Press. 2000.

[9] D. Halliday *et al. Physics*, 4th Ed. Vol. 4. Joh Wiley and Sons, Inc. 1992.

[10] S. Kumar. "A Proposal for Electriacally Levitating Micromotors," *Sensors and Actuators A*, Vol. 24 pp. 141-149 1990.

[11] J. Jones and R. Dugan. *Engineering Thermodynamics* 1st Ed. Prentice Hall College Division. 1995.

[12] J. Judy *et al.* "Magnetic Microactuation of Polysilicon Flexure Structures," Solid-State Sensor and Actuator Workshop. 1994.

[13] H. Martin. *The Design of Hydraulic Components and Systems*, Ellis Horwood. 1995.

[14] Maxim Integrated Products, http://www.maximic.com. 2002.

[15] T. Niino *et al.* "Dual Excitation Electrostatic Stepping Motor," Electrical Engineering in Japan **119(3)**: 94-103 1997

[16] T. Niino *et al.* "X-Y Positioner Driven by Electrostatic Motor," IEEE, 1996.

[17] J. Peirs *et al.* "The 'True' Power of SMA Micro-Actuation," Micromechanics Europe Workshop, pp.**217-220**. 2001.

[18] E. Purcell. *Electricity and Magnetism Vol. 2*, 2nd Ed. McGraw-Hill. 1985

[19] W. Purves *et al. Life: The Science of Biology* 5th Ed. W.H. Freeman and Company. 1998.

[20] J. Taylor, Media Lab, Massachusetts Institute of Technology. 2002.

[21] R. Valentine. *Motor Control Electronics Handbook.* McGraw-Hill. 1998.

[22] B. Wagner *et al.* "Microactuators with moving magnets for linear, torsional, or multiaxial motion," *Sensors and Actuators A (Physical)*, Vol. A32, no. 1-3, pp. 598-603, 1992.

[23] F. White. *Fluid Mechanics*, 4th Ed. McGraw-Hill. 1999

[24] A. Wissner-Gross, Department of Physics, Massachusetts Institute of Technology. 2001.

[25] A. Yamamoto *et al.* "Development of a controller for high-power electrostatic motor," *Electrical Engineering in Japan* Vol. 133 no. 4 pp. 91-99, 2000.

[26] A. Yamamoto *et al.* "A High-Power Electrostatic Motor Using Skewed Electrodes," *Electrical Engineering in Japan.* Vol. 25 no. 3 pp. 50-58, 1998.